4 Resultados

(Esta página está intencionadamente en blanco)

En este capítulo se presentan los resultados obtenidos al abordar los objetivos propuestos en esta memoria. Tal y como se ha señalado en la introducción, en la presente tesis han sido objeto de investigación las interacciones débiles que pueden establecer las bases nitrogenadas de los ácidos nucleicos. Los resultados referentes a cada una de estas interacciones se muestran en diferentes bloques.

4.1 Interacciones π-catión[1-3]

Son interacciones relativamente fuertes y bastantes específicas, que tiene un papel importante en el reconocimiento molecular y deberían considerarse una fuerza de unión no covalente común e importante. Así se ha descrito su importancia en un gran número de sistemas, como la formación de complejos *host-guest* (receptores artificiales), la estabilización de estructuras proteicas (interacciones de las cadenas laterales en proteínas) y en diversos procesos biológicos, como mecanismos de catálisis, unión ligando-receptor, el paso de iones a través de canales, etc.

La interacción π-catión es fundamentalmente electrostática, y se da entre especies cargadas positivamente (un catión) y sistemas con distribución electrónica de tipo π. Especialmente importantes son las interacciones π entre anillos bencénicos y metales alcalinos como los iones Na^+ y K^+. Interacciones similares son posibles en otros anillos aromáticos incluyendo las nucleobases del ADN[4].

En el apartado 4.1.1 se presenta un estudio sistemático de la contribución de los efectos de polarización a las interacciones π-cation entre el sodio y una serie de sistemas aromáticos modelo. Para ello se ha utilizado un programa desarrollado en nuestro grupo, MOPETE, que permite calcular el potencial generalizado de interacción molecular con polarización (GMIPp), una aproximación también desarrollada por nuestro grupo[5]. También se analiza la posibilidad de introducir los efectos de polarización en los

"índices de reactividad", los cuales son usados para la predicción de la fuerza de las interacciones π-catión.

En el apartado 4.1.2 se examinan las principales características de la interacción π-catión en términos de las propiedades topológicas de la densidad de carga electrónica. Este análisis ha sido realizado para el sodio con una serie de derivados del benceno y anillos aromáticos de cinco miembros, usando la teoría *Atoms in molecules* (AIM)[6]. También se ha caracterizado la interacción del benceno con una variedad de sistemas químicos que incluye cationes y moléculas neutras, con la misma metodología.

4.1.1 Is polarization important in cation-π interactions?

Elena Cubero, F. Javier Luque & Modesto Orozco

Proc. Natl. Acad. Sci. USA. **1998**, *95*, 5976-5980

(Esta página está intencionadamente en blanco)

Proc. Natl. Acad. Sci. USA
Vol. 95, pp. 5976–5980, May 1998
Chemistry

Is polarization important in cation-π interactions?

ELENA CUBERO*, F. JAVIER LUQUE†‡, AND MODESTO OROZCO*‡

*Departament de Bioquímica, Facultat de Química, Universitat de Barcelona, Martí i Franquès 1, Barcelona 08028, Spain; and †Departament de Fisicoquímica, Facultat de Farmàcia, Universitat de Barcelona, Avgda Diagonal s/n, Barcelona 08028, Spain

Edited by Kenneth B. Wiberg, Yale University, New Haven, CT, and approved March 19, 1998 (received for review December 19, 1997)

ABSTRACT **The importance of cation-> aromatic polarization effects on cation-π interactions has been explored. Theoretical calculations demonstrate that polarization is a large contribution to cation-aromatic interactions, and particularly to cation-π interactions. For a series of compounds with a similar aromatic core, polarization is constant and makes small influence in the relative cation-binding energies. However, when the aromatic core changes polarization contributions might be very different. We found that the generalized molecular interaction potential with polarization is a very fast and powerful tool for the prediction of cation binding of aromatic compounds.**

Cation-π is a strong, and quite specific, interaction, which plays a key role in molecular recognition (for an excellent review see ref. 1). Thus, cation-π interactions are relevant in host-guest complexes (1–5). In addition, they are common in protein structure (6–8), where these interactions seem to be related with general mechanisms of substrate-enzyme binding (8–12) and probably with some catalytic processes (13–16). Finally, Dougherty and coworkers (17, 18) recently have suggested that these interactions are essential for the recognition and action of ion channels.

Cation-π complexes involve aromatic molecules having large and well-defined π-electron distributions, and the cations lie perpendicular to the aromatic plane. Dougherty and coworkers (1, 7, 18, 19) have shown that, in the case of nonpolarizable cations such as Na^+, the preferential binding to different aromatic compounds can be explained from electrostatic considerations. Particularly, for a series of 11 derivatives of benzene, they found an excellent correlation ($r = 0.991$, slope = 1.01, intercept = 11.6 kcal/mol) between the self-consistent field (SCF) binding energies and the molecular electrostatic potential (MEP; Eq. **1**) at the SCF-optimized position of the Na^+ in the complex (19). More interesting, when the MEP was computed at a common position for all of the molecules (2.47 Å above the aromatic ring), the correlation with the SCF binding energy was also excellent ($r = 0.992$, slope = 1.04, intercept = 12.3 kcal/mol). This finding suggests that a simple MEP calculation can provide very accurate estimates of the relative values of cation binding energy for a given series of aromatic compounds (18, 19).

$$\mathrm{MEP} = \sum_{\mathrm{A}} \frac{Z_{\mathrm{A}}}{|R_{\mathrm{B}} - R_{\mathrm{A}}|} - \sum_{\mathrm{i}}^{\mathrm{occ}} \sum_{\mu} \sum_{\mathrm{v}} \mathrm{c}_{\mu\mathrm{i}}\, \mathrm{c}_{\mathrm{vi}} \left\langle \phi_{\mu} \left| \frac{1}{|R_{\mathrm{B}} - \mathrm{r}|} \right| \phi_{\mathrm{v}} \right\rangle, \quad [1]$$

where R_{B} and R_{A} stands for the positions of the cation and nuclei, and c stands for the coefficients of atomic orbitals in the molecular orbital-linear combination atomic orbitals (MO-LCAO) approximation.

The pure electrostatic model seems very useful for a qualitative description of cation-π interactions. However, the electrostatic component of the cation-π interaction energy is always larger (in absolute terms) than the MEP value. Therefore, other interactions are involved in the formation of cation-π complexes. For the particular case of Na^+, the charge transfer is expected to be small. Indeed, the polarization of the π-electron system by the cation will have a significant contribution, whereas the reverse effect is expected to be sensibly lower. In fact, the relevance of polarization effects in cation-π interactions has been previously emphasized by Kollman and Caldwell (20) by using classical force-field calculations.

In this paper we present a systematic quantum mechanical study on the contribution of polarization effects to cation-π interactions. We also analyze the possibility to introduce these polarization effects into "reactivity indexes," which are used for the prediction of the strength of cation-π interactions.

METHODS

The study is performed by using a perturbational approach to compute the polarization energy. Particularly, we analyze the suitability of the recently developed generalized molecular interaction potential with polarization (GMIPp; refs. 21–23) as an improved computational generalization of the MEP for the *a priori* description of chemical reactivity. Three terms contribute to the interaction energy in the GMIPp: (*i*) an electrostatic term identical to the MEP, (*ii*) a classical dispersion-repulsion term (refs. 22 and 23; §), and (*iii*) a polarization term derived from perturbational theory (21–23). Let us note that the polarization effects are estimated at a reduced computational effort and that the perturbational and SCF values of the polarization energy are very similar (ref. 23; ¶). For the case of the interaction with Na^+, the GMIPp is given by Eq. **2**.

The publication costs of this article were defrayed in part by page charge payment. This article must therefore be hereby marked "*advertisement*" in accordance with 18 U.S.C. §1734 solely to indicate this fact.

© 1998 by The National Academy of Sciences 0027-8424/98/955976-5$2.00/0
PNAS is available online at http://www.pnas.org.

This paper was submitted directly (Track II) to the *Proceedings* office.
Abbreviations: SCF, self-consistent field; MEP, molecular electrostatic potential; GMIPp, generalized molecular interaction potential with polarization; E_{ele}, electrostatic binding energy; E_{pol}, polarization binding energy; E_{tot}, total binding energy.
‡To whom reprint requests should be addressed.
§C and D were computed with geometrical combinatorial rules: $C_{\mathrm{AB}} = 4\varepsilon_{\mathrm{AB}}\sigma_{\mathrm{AB}}{}^{12}$ and $D_{\mathrm{AB}} = 4\varepsilon_{\mathrm{AB}}\sigma_{\mathrm{AB}}{}^{6}$, where $\varepsilon_{\mathrm{AB}} = (\varepsilon_{\mathrm{A}}\,\varepsilon_{\mathrm{B}})^{0.5}$ and $\sigma_{\mathrm{AB}} = (\sigma_{\mathrm{A}}\,\sigma_{\mathrm{B}})^{0.5}$. van der Waals parameters (ε, σ) for *C*, *N*, and *H* were taken from an in-house quantum mechanical–molecular mechanical (QM-MM) parametrization (*H*: $\varepsilon = 0.0116$, $\sigma = 2.272$; *C*: $\varepsilon = 0.0488$, $\sigma = 3.77$, *N*: $\varepsilon = 0.0521$, $\sigma = 3.225$), and the rest of van der Waals parameters for aromatic compounds were taken from the optimized potentials for liquid simulations (OPLS) force-field (24). Parameters for Na^+ were taken from Aqvist's parameters (25). Parameters for boron were taken equal to those of carbon.
¶As an example, the SCF estimates (kcal/mol) of cation-π interactions at the optimum SCF distances are −9.3 for benzene and −8.9 for

$$\text{GMIPp} = \sum_{A} \frac{Z_A}{|R_B - R_A|} - \sum_{i}^{occ} \sum_{\mu} \sum_{\nu} c_{\mu i}\, c_{\nu i} \left\langle \phi_\mu \left| \frac{1}{|R_B - r|} \right| \phi_\nu \right\rangle + \sum_{A} \left(\frac{C_{AB}}{|R_B - R_A|^{12}} - \frac{D_{AB}}{|R_B - R_A|^{6}} \right) + \sum_{j}^{vir} \sum_{i}^{occ} \frac{1}{\varepsilon_i - \varepsilon_j} \left\{ \sum_{\mu} \sum_{\nu} c_{\mu i}\, c_{\nu j} \left\langle \phi_\mu \left| \frac{1}{|R_B - r|} \right| \phi_\nu \right\rangle \right\}^2, \quad [2]$$

where C_{AB} and D_{AB} are the van der Waals interaction parameters[§], and ε_i denotes the energy of molecular orbital i.

Calculations were performed by using the HF/6–31G(d,p) geometries and wavefunctions, because this level of theory provides (probably because of fortuitous error cancellation) very accurate values of the cation-π binding energy (refs. 1, 7, 18, and 19; [‖]). Empirical van der Waals parameters were used[§]. In all calculations the Na^+ was considered as a classical nonpolarizable particle.

Wavefunction calculations have been performed by using the GAUSSIAN 94 computer program (27); MEP and GMIPp calculations were performed with the MOPETE program (28). All calculations have been carried out on the IBM-SP2 computer of the Centre de Supercomputació de Catalunya and on workstations in our laboratory.

RESULTS AND DISCUSSION

We first explored the profiles for the electrostatic (E_{ele}), polarization (E_{pol}), and total (E_{tot}) binding energies when a Na^+ approaches a benzene molecule. Three orientations were considered (see Fig. 1): (*i*) along the middle of a C-C bond (*x* orientation), (*ii*) along the C-H bond (*y* orientation), and (*iii*) perpendicular to the center of the aromatic ring (*z* orientation). In all cases we determined the "hard particle radius," which was defined as the point where dispersion and repulsion cancel each other. Then, we computed E_{ele}, E_{pol}, and E_{tot} there and in points closer to and farther away from the molecule.

The energy profiles (see Fig. 2) provide insight into the nature of cation-π interactions. At very short distances the repulsive term dominates the interaction, whereas the electrostatic component is the leading term at very large distances. At intermediate values (near the hard sphere radius) the magnitude of E_{ele} and E_{pol} is in general similar. As expected, the electrostatic term is positive for *x* and *y* orientations, whereas it is large and negative for the approach along the *z* axis. The polarization term is always negative and seems to follow a r^{-3} dependence, compared with well-known r^{-1} dependence of the electrostatic term.

When the Na^+ approaches along the *x* and *y* axis, the polarization energy is larger (in absolute value) than the electrostatic term for distances shorter than the hard sphere radius plus 0.8 (*y* axis) or 1.2 (*x* axis) Å. This suggests that the energy profile for the cation approach to the benzene in the aromatic plane is not fully repulsive, as noted in the minima in the E_{tot} profiles of −3.8 (at −0.6 Å; around 4 Å from the center of the ring) and −1.5 (at −0.4 Å; around 4.6 Å from the center of the ring) kcal/mol for the *x* and *y* orientations. The existence of these minima was verified by performing SCF calculations, which provided binding energies of −4.6 and −2.0 kcal/mol, respectively. It then is clear that the large magnitude of the aromatic polarization stabilizes the in-plane approach of cations in spite of the strong electrostatic repulsion.

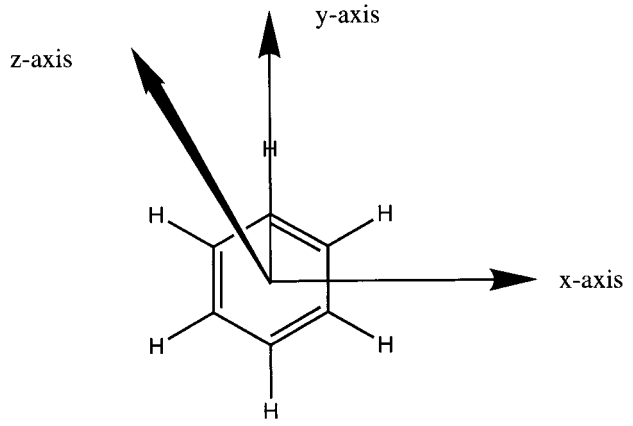

FIG. 1. Orientations of cation-aromatic interactions in the study. The *z* axis corresponds to the cation-π interaction.

The approach of the cation along the *z* axis is clearly favored by the electrostatic term. This component is greater (in absolute terms) than the polarization for distances larger than −1.3 Å. The polarization energy is 44% the magnitude of the electrostatic energy at the hard sphere radius, and 70% the magnitude of the electrostatic term at the optimum distance of 2.47 Å (around −0.8 Å). Note in Fig. 2 that the SCF and GMIPp optimum Na^+-benzene distances are very similar (within 0.1 Å). It is then clear that polarization has a nonnegligible contribution to the total cation-π binding energy.

Inspection of E_{pol} profiles shows that at large distances E_{pol} is very similar irrespectively of the cation orientation. At intermediate distances the *x* orientation leads to the largest polarization, whereas the smallest effects are found for the *z* orientation, but the differences are in any case small. At the hard sphere radius E_{pol} is −5.2 (*x* axis), −4.3 (*y* axis), and −4.2 (*z* axis) kcal/mol. At inner distances the *y* orientation provides the largest polarization, as noted in the values of E_{pol} 95 at a distance of −1.0 Å: −16.0 (*x* axis), −16.5 (*y* axis), and −13.2 kcal/mol (*z* axis). In summary, polarization favors the in-plane approach of cations, but the small difference with respect to the *z*-axis orientation cannot revert the electrostatic preference for the perpendicular orientation.

After examining the dependence of E_{ele}, E_{pol}, and E_{tot} on orientation factors, we explored the polarization contribution to the interaction of Na^+ for a series of 16 aromatic compounds (see Fig. 3). This also allowed us to explore the suitability of the GMIPp as an alternative to the MEP for the *a priori* description of cation-π interactions. Following Dougherty and coworkers (18, 19), we computed the MEP and the GMIPp at 2.47 Å above the aromatic ring and compared these values with the optimum SCF interaction energies[**]. The results in Table 1 point out the importance of the polarization component, which is in general similar to the electrostatic one, and for six of the 16 compounds it is even larger than the electrostatic term. The polarization energy is mainly related to the size of

furan, which compare with the GMIPp values of −9.9 and −9.1 kcal/mol, respectively.

[‖]Single point calculations (HF/6–31G(d,p) geometries) were performed for the Na^+. . . Phe dimer at the MP2/6–311++G(2d,p) level. The interaction energy was (after basis set superposition error correction) −22.0 kcal/mol (−21.2 if the Na^+ is fixed at 2.47 Å above the aromatic ring). These values compare well with the HF/6–31G(d) values (−27.1 kcal/mol). Experimental enthalpy of interaction determined by Guo *et al.* (26) for this system is −28 kcal/mol.

[**]Geometry optimization leads to optimum distances that can be different from the "average" value of 2.47 Å, as noted previously by Dougherty and coworkers (18, 19). However, the difference between the optimized distance and 2.47 Å is less than 0.05 Å for all molecules, except for compounds 10, 11, and 12 (optimum distances of 2.53 Å, 2.54 Å, and 2.59 Å, respectively). In addition to the situation for compounds 15 and 16 (see text), geometry optimization can lead to slight deviations of the Na^+ with respect to the center of the aromatic ring. The largest deviations are found for compounds 3 (0.20 Å), 14 (0.20 Å), and 4 (0.19 Å). Finally, as noted in ref. 18, molecules containing heteroatoms might have an additional minima corresponding to a cation-σ interaction.

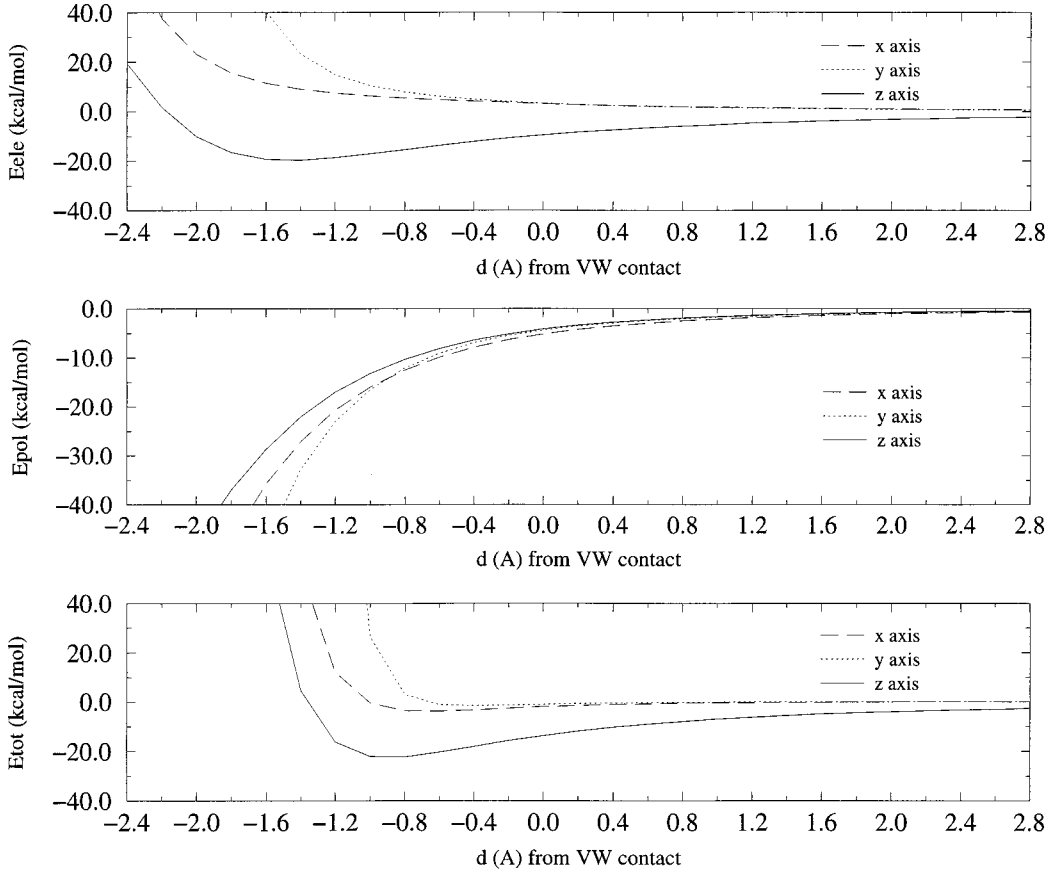

FIG. 2. GMIPp energy profiles for the approach of Na^+ to benzene (*x* axis: dotted line; *y* axis: dashed line; *z*-axis: solid line). (*Top*) Electrostatic energy. (*Middle*) Polarization energy. (*Bottom*) Total energy. All the values are in kcal/mol. Distances (in Å) are referred in all cases to the hard sphere radius (see text). Hard sphere radii are: 4.58 (*x* axis), 4.97 (*y* axis), and 3.24 Å (*z* axis).

the aromatic system, with little dependence on the nature of the substituents. Thus, for benzene and their substituted derivatives E_{pol} ranges from −10 to −11 kcal/mol, a value that is around 1 kcal/mol larger (in absolute terms) to those found for five-membered rings. Larger aromatic rings provide larger values of E_{pol}. Thus, the E_{pol} for indole is −12.4, and for the 10-membered rings of naphthalene and azulene amounts to −13.7 and −16.2 kcal/mol.

Inspection of the benzene series shows that the introduction of electron withdrawing groups leads to a dramatic reduction of the electrostatic energy, as noted by Dougherty and coworkers (18, 19), whereas E_{pol} shows little variation (see Table 1). Accordingly, the nature of the cation-π interaction changes from mostly electrostatic to be dominated by polarization effects. Thus, E_{pol} is 55% of E_{ele} for aniline, 102% for the fluoro derivative, 345% for the cyano derivative, and more than 3,000% for the tri-fluoro derivative. Therefore, even though a pure electrostatic model is not able to reproduce accurately the cation-π interaction, it can provide excellent relative values for a series of aromatic compounds of similar size, in agreement with previous studies (18).

To analyze the reliability of the electrostatic model on the size of the aromatic system, we examined the correlation between SCF and MEP values. The results (see Fig. 4*A*) show that the electrostatic model performs well, but obviously worse than on application to the series of benzene derivatives. Thus, the model explains 93% of the variance of the results, the intercept is −11.6 kcal/mol, and the slope is 1.08. However, a detailed inspection of the results in Table 1 allows us to detect some of the most clear shortcomings of the electrostatic model. For instance, it predicts benzene as better cation binder than naphthalene, which is in disagreement with SCF results. Similarly, the boron derivative of benzene and furan show the same electrostatic energy, but the first binds Na^+ better according to the SCF values. Another example is furnished by the cation binding to indole and azulene, which is predicted to be better for indole by the MEP, whereas the opposite trend is found at the SCF level. In all of these cases the polarization varies sensibly and modulates the total interaction energy.

The performance of the GMIPp model can be examined from the correlation analysis given in Fig. 4*B*, which shows the superiority of this computational tool. Thus, 99% of the variance in the SCF results is reproduced by the model, the slope is 0.984 and the intercept amounts to −5.0 kcal/mol. The value of the intercept reflects the basis set superposition error (BSSE), which was not corrected in the SCF values following Dougherty's suggestions (18, 19) (for instance, the BSSE for benzene is −1.8 kcal/mol, and for naphthalene is −1.6 kcal/mol), and the remaining 60% of the intercept might arise from uncertainties in the classical evaluation of the repulsion contribution (the van der Waals component is around 3 kcal/mol), to Na^+ polarization, and obviously to charge transfer effects. In fact, Bader's analysis (29) for the benzene-Na^+ system shows that around 0.05 electrons are transferred from benzene to Na^+, which can account for a few kcal/mol of stabilization in the complex formation††.

Overall, the improvement of the GMIPp with respect to the MEP is clear, as shown by the increase of ≈6% in the

††Correlations were performed from the GMIPp at 2.47 Å above the aromatic ring instead of the SCF or GMIPp optimized geometry. Calculations performed by using these optimized geometries provided almost identical results to those obtained for the frozen geometry, as previously reported for MEP calculations by Dougherty and coworkers (18, 19).

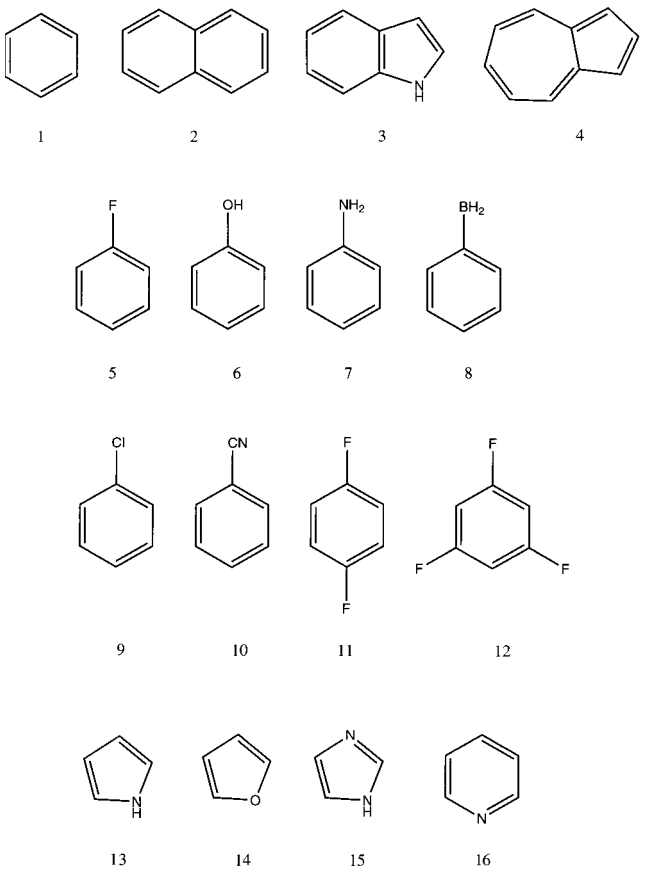

FIG. 3. Aromatic structures considered in this study.

descriptive ability of the model, a reduction of ≈7% in the deviation of the slope from the ideal value, and the notable reduction of ≈6.5 kcal/mol in the systematic deviation noted by the intercept. Furthermore, the GMIPp reproduces the differences in Na^+ binding to benzene/naphthalene, furan/Phe-BH_2, and indole/azulene. Computationally, the GMIPp requires a limited increase in computer time compared with the MEP, because the recomputation of the wavefunction is not necessary, and E_{pol} is evaluated by using the same mono-

Table 1. Electrostatic (MEP) energy, polarization energy, and total energy ($GMIP_p$ and SCF) for the interaction of Na^+ with several aromatic systems

Molecule	E_{ele}(MEP)	E_{pol}	$GMIP_p$	E(SCF)
1	15.0	9.9	21.9	27.1
2	14.2	13.7	25.1	28.7
3	18.8	12.4	28.2	32.6
4	17.1	16.2	29.5	34.1
5	9.8	10.0	16.8	22.0
6	14.0	10.3	21.3	26.9
7	19.3	10.7	27.0	31.8
8	11.1	11.1	19.2	24.4
9	9.3	10.9	17.1	21.5
10	3.3	11.4	11.7	15.7
11	4.6	10.1	11.6	16.8
12	−0.3	10.3	6.9	12.4
13	18.1	9.7	24.4	29.6
14	11.2	9.2	16.7	21.0
15	11.2	9.4	17.3	21.0
16	8.4	9.6	15.2	20.0

MEP, E_{pol}, and $GMIP_p$ were computed by placing the Na^+ at 2.47 Å above the aromatic ring. The SCF values were computed by optimizing the complex geometry. All the values are in kcal/mol. (See Fig. 3.)

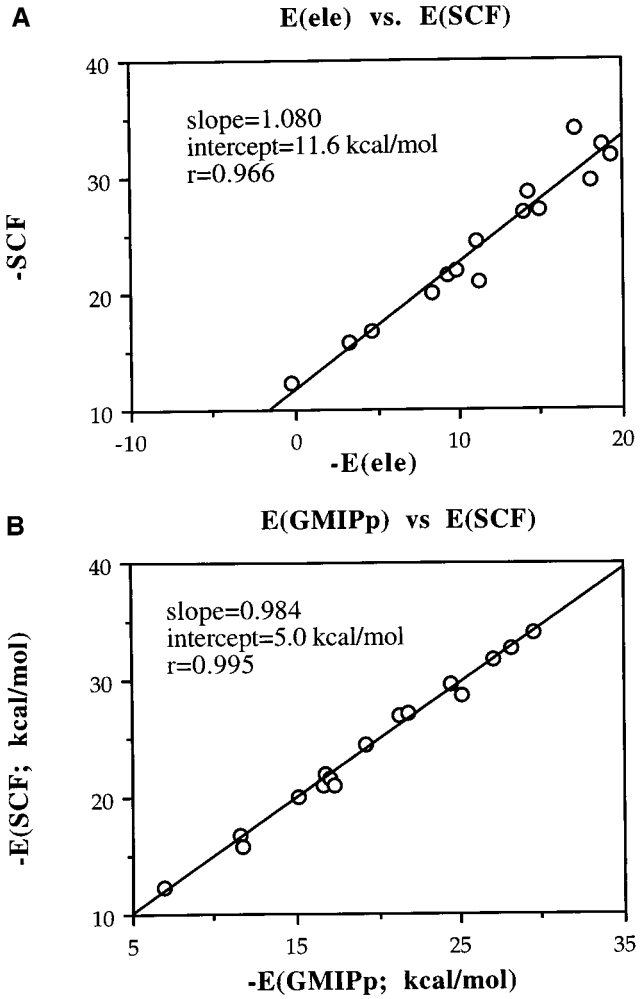

FIG. 4. Correlations between SCF and MEP (*A*) and GMIPp (*B*) values.

electron integrals involved in the calculation of the MEP. Furthermore, because the GMIPp is based on perturbational treatment, it provides a natural partitioning of the interaction energy into intuitive components, without the uncertainties derived from basis set superposition error. All of these results suggest the GMIPp as a more precise alternative to the MEP for the quantitative analysis of cation-π interactions, specially in cases where aromatic systems of different sizes are to be studied.

This work has been supported by the Spanish Dirección General de Investigación Cientifica y Técnica (PB96-1005), and by the Centre de Supercomputació de Catalunya (CESCA, Molecular Recognition Project).

1. Ma, J. C. & Dougherty, D. A. (1997) *Chem. Rev.* **97,** 1303–1324.
2. Shepodd, T. J., Petti, M. A. & Dougherty, D. A. (1986) *J. Am. Chem. Soc.* **108,** 6085–6087.
3. Shepodd, T. J., Petti, M. A. & Dougherty, D. A. (1988) *J. Am. Chem. Soc.* **110,** 1983–1985.
4. Petti, M. A., Shepodd, T. J. & Dougherty, D. A. (1988) *J. Am. Chem. Soc.* **110,** 6825–6840.
5. Arnecke, R., Böhmer, V., Cacciapaglia, R., Cort, A. D. & Mandolini, L. (1997) *Tetrahedron* **53,** 4901–4908.
6. Burley, S. K. & Petsko, G. A. (1986) *FEBS Lett.* **203,** 139–143.
7. Dougherty, D. A. (1996) *Science* **271,** 163–168.
8. Scrutton, N. A. & Raine, A. R. C. (1996) *Biochem. J.* **319,** 1–8.
9. Sussman, J. L., Harel, M., Frolow, F., Oefner, C., Goldman, A., Toker, L. & Silman, L. (1991) *Science* **256,** 7781–7785.
10. Ortiz, A. R., Pisabarro, T., Gallego, J. & Gago, F. (1992) *Biochemistry* **31,** 2887–2896.

11. Ortiz, A. R., Pisabarro, T., Gallego, J. & Gago, F. (1993) *J. Med. Chem.* **36,** 1866–1879.
12. Galzi, J. L., Revah, F., Bessis, A. & Changeux, J. P. (1992) *Annu. Rev. Pharmacol.* **31,** 37–72.
13. Stauffer, D. A., Barrans, J. R. E. & Dougherty, D. A. (1990) *Angew. Chem. Int. Ed. Engl.* **29,** 915–918.
14. McCurdy, A., Jiménez, L., Stauffer, D. A. & Dougherty, D. A. (1992) *J. Am. Chem. Soc.* **114,** 10314–10321.
15. Shi, Z., Butel, C. J. & Griffin, J. H. (1994) *Proc. Natl. Acad. Sci. USA* **91,** 7370–7374.
16. Heginbotham, L. & MacKinnon, R. (1992) *Neuron* **8,** 483–491.
17. Kumpf, R. A. & Dougherty, D. A. (1993) *Science* **261,** 1708–1710.
18. Mecozzi, S., West, A. P. & Dougherty, D. A. (1996) *Proc. Natl. Acad. Sci. USA* **93,** 10566–10571.
19. Mecozzi, S., West, A. P. & Dougherty, D. A. (1996) *J. Am. Chem. Soc.* **118,** 2307–2308.
20. Caldwell, J. W. & Kollman, P. A. (1995) *J. Am. Chem. Soc.* **117,** 4177–4178.
21. Francl, M. M. (1985) *J. Phys. Chem.* **89,** 428–434.
22. Orozco, M. & Luque, F. J. (1996) in *Molecular Electrostatic Potentials: Concepts and Applications*, eds. Murray, J. S. & Sen, K. (Elseiver, Amsterdam), Vol. 3, pp. 181–218.
23. Luque, F. J. & Orozco, M. (1998) *J. Comp. Chem.*, in press.
24. Jorgensen, W. L. & Tirado-Rives, J. (1988) *J. Am. Chem. Soc.* **110,** 1657–1666.
25. Aqvist, J. (1990) *J. Phys. Chem.* **94,** 8021–8024.
26. Guo, B. C., Purnell, J. W. & Castleman, A. W. (1990) *Chem. Phys. Lett.* **168,** 155–160.
27. Frisch, M. J., Trucks, G. W., Schlegel, H. B., Gill, P. M. W., Johnson, B. G., Robb, M. A., Cheeseman, J. R., Keith, T. A., Petersson, G. A., Montgomery, J. A., *et al.* (1995) GAUSSIAN 94, Rev. A.1 (Gaussian, Pittsburgh).
28. Luque, F. J. & Orozco, M. (1997) MOPETE (University of Barcelona, Spain).
29. Bader, R. F. W., Carroll, M. T., Cheeseman, J. R. & Chang, C. (1987) *J. Am. Chem. Soc.,* **109,** 7968–7979.

(Esta página está intencionadamente en blanco)

4.1.2 A topological analysis of electron density in cation-π complexes

Elena Cubero, Modesto Orozco & F. Javier Luque

J. Phys. Chem. A. **1999**, *103*, 315-321

(Esta página está intencionadamente en blanco)

A Topological Analysis of Electron Density in Cation−π Complexes

E. Cubero,[†] M. Orozco,*[,†] and F. J. Luque*[,‡]

Departament de Bioquímica i Biologia Molecular, Facultat de Química, Universitat de Barcelona, Martí i Franqués 1, 08028 Barcelona, Spain, and Departament de Fisicoquímica, Facultat de Farmàcia, Universitat de Barcelona, Av. Diagonal s/n, 08028 Barcelona, Spain

Received: August 17, 1998; In Final Form: October 30, 1998

A topological analysis of the electron density in cation−π complexes is presented. Calculations are performed for complexes involving the interaction of the Na^+ ion with a variety of six- and five-membered aromatic rings, as well as for the interaction of benzene with diverse cations and hydrogen-bonded neutral molecules. The results reveal the existence of great differences in the topological features of the electron density, which reflect the profound influence of the substituents attached to the aromatic core or of the presence of heteroatoms and fused rings. Nevertheless, with exception of the complexes involving five-membered rings, there are strong relationships between the charge density at the cage critical points and both the energetic and geometrical parameters of the complexes. These relationships allow us to generalize the concept of bond order−bond length found for other intermolecular interactions.

Introduction

Cation−π interactions are recognized to be strong noncovalent binding forces with a large importance in a wide range of systems, including small organic molecules, supramolecules and biochemical macromolecules.[1−6] Much of the information on cation−π interactions comes from crystallographic studies, but further support is given by data in the gas phase and in solution.[1,7] Most studies have addressed the nature and energetics of cation−π interactions.[8−15] The results showed that for complexes of simple ions, i.e., Li^+ or Na^+, calculations at the Hartree−Fock level are adequate, but correlation effects can be quantitatively important for complexes involving cations such as $N(CH_3)_4^+$. The cation−π interaction is in general dominated by electrostatic and cation-induced polarization. As we have recently shown,[15] these two terms explain around 99% of the variance in the binding energies for a series of 16 Na^+−π complexes that includes both six- and five-membered aromatic rings.

The aim of this study is to examine the main features of cation−π interactions in terms of the topological properties of the electron charge density. Such an analysis can be done efficiently using the theory of "atoms in molecules".[16,17] This approach has been successfully used to characterize the formation of hydrogen bonds in a variety of molecular complexes.[18−25] Moreover, several studies have shown a clear relationship between the topological properties of the charge density in hydrogen-bonded complexes with both the interaction energy and the internuclear distance of the complexes.[26,27] The theory has been also used for the understanding of the cation complexation to the heteroatom lone electron pairs in heterocycles, like the binding of Li^+ to the nitrogen atom in azoles and azines,[28,29] but to our knowledge it has not yet been used to characterize cation−π interactions.

In this paper we have examined the interaction of Na^+ with a series of derivatives on benzene. Indeed, we have extended such an analysis to the interaction of Na^+ with five-membered aromatic rings, as well as to the interaction of benzene with a variety of chemical systems including both cations and hydrogen-bonded neutral molecules. Particularly, we have investigated the relationship of the topological properties with both the energetics and geometrical features in these complexes. The results evidence the complexity of the cation−π interaction as far as the topology of the electron density is concerned, but they also show the existence of relationships between the topological features and the energetics of cation−π complexes.

Methods

Topological Properties of Electron Density. A brief review of some relevant concepts within Bader's topology analysis is appropriate to facilitate the analysis of the results (the reader is addressed to refs 16 and 17 for a more comprehensive explanation). The existence of a bond path linking two nuclei in an equilibrium structure implies that the two atoms are bonded to one another. Such a path is characterized by the bond critical point, which is the point of minimum charge density along the bond, but a maximum along the directions perpendicular to the bond path. A critical point can be characterized by the number of zero eigenvalues of the associated Hessian matrix, which determines its rank, and the algebraic sum of their signs, which determine its signature. A bond critical point is denoted as (3, −1) and has one positive (λ_3) and two negative (λ_1, λ_2) curvatures, one (λ_3) associated with the charge density along the bond path and the other (λ_1, λ_2) perpendicular to the bond path. An interesting feature is the ellipticity (ϵ), which is defined as $\lambda_1/\lambda_2 - 1$ and gives a measure of the extent to which electron density is accumulated in a given plane. Thus, the ellipticity for a cylindrical symmetrical bond like C−C in ethane is 0.0, and it amounts to around 0.45 for ethene. There can be other types of nondegenerate critical points: (3, −3), (3, +1), and (3, +3). The first corresponds to position of local maxima of the charge density (the nuclei). The two other types occur as a consequence of particular geometrical arrangements of bond paths and define elements of molecular structure. If the bond

* To whom correspondence should be sent.
[†] Facultat de Química.
[‡] Facultat de Farmàcia.

10.1021/jp983382s CCC: $18.00 © 1999 American Chemical Society
Published on Web 01/14/1999

TABLE 1: Interaction Energies (E, kcal/mol), Equilibrium Distances (R_e, Å), and Selected Electron Density Topological Properties for $Na^+-\pi$ Complexes of Benzene Derivatives, Pyridine, Naphthalene, and Indole

compound	E	R_e	CP[a]	n	$10^2\rho$	$10^2\nabla^2\rho$	r_{cp}
H	−27.1	2.45	(3, −1)	6	0.991	4.682	1.41
			(3, +1)	6	0.989	4.671	1.41
			(3, +3)	1	0.791	4.115	1.19
NH_2	−31.8	2.43	(3, −1)	1	1.094	5.225	1.41
			(3, +1)	1	0.940	4.435	1.38
			(3, +3)	1	0.816	4.221	1.17
OH	−26.9	2.46	(3, −1)	1	1.093	5.175	1.42
			(3, +1)	1	0.867	4.071	1.40
			(3, +3)	1	0.780	3.994	1.20
BH_2	−24.4	2.46	(3, −1)	1	0.974	4.595	1.42
			(3, −1)	2	0.977	4.560	1.42
			(3, +1)	1	0.953	4.468	1.41
			(3, +1)	2	0.969	4.593	1.41
			(3, +3)	1	0.777	4.024	1.20
F	−22.0	2.50	(3, −1)	1	1.019	4.735	1.45
			(3, +1)	1	0.813	3.841	1.43
			(3, +3)	1	0.733	3.739	1.23
Cl	−21.5	2.49	(3, −1)[b]	1	0.942	4.392	1.43
			(3, −1)[c]	1	0.911	4.376	1.44
			(3, +1)	2	0.911	4.375	1.43
			(3, +3)	1	0.752	3.878	1.23
1,3-diF	−16.8	2.54	(3, −1)	2	0.846	3.891	1.48
			(3, +1)	2	0.828	3.860	1.47
			(3, +3)	1	0.690	3.478	1.27
CN	−15.7	2.54	(3, −1)[b]	1	0.851	3.896	1.47
			(3, −1)[c]	1	0.840	4.067	1.47
			(3, −1)	2	0.852	3.906	1.47
			(3, +1)[d]	2	0.851	3.891	1.46
			(3, +1)[e]	2	0.837	4.008	1.46
			(3, +3)	1	0.692	3.578	1.26
1,3,5-triF	−12.4	2.60	(3, −1)	3	0.774	3.484	1.53
			(3, +1)	3	0.742	3.468	1.49
			(3, +3)	1	0.634	3.142	1.31
pyridine	−20.0	2.51	(3, −1)	2	0.915	4.191	1.46
			(3, +1)[b]	1	0.904	4.147	1.45
			(3, +1)[f]	1	0.789	4.080	1.42
			(3, +3)	1	0.714	3.882	1.25
naphthalene	−28.7	2.43	(3, −1)	2	1.041	4.854	1.42
			(3, +1)[g]	1	0.957	4.674	1.39
			(3, +1)[h]	1	1.004	4.794	1.39
			(3, +3)	1	0.794	4.105	1.18
indole	−32.6	2.41	(3, −1)	1	1.220	5.856	1.38
			(3, +1)	1	0.892	4.308	1.38
			(3, +3)	1	0.810	4.204	1.17

[a] The electron density (ρ, atomic units) and its Laplacian ($\nabla^2\rho$, atomic units) at the (3, −1), (3, +1) and (3, +3) critical points (CP) originated upon complexation are given, as well as the total number (n) of each CP in the complex and the distance (r_{cp}, Å) from the aromatic ring to the CP. [b] Near C4. [c] Near C1. [d] Near C3 (C5). [e] Near C2 (C6). [f] Near N. [g] Near C2−C3. [h] Near C9−C10.

paths are linked so as to form a ring of bonded atoms, a (3, +1) ring critical bond is formed in the interior of the ring. If the bond paths are arranged as to enclose the interior of a molecule with ring surfaces, then a (3, +3) cage critical point is found in the interior of the cage, the charge density being a local minimum at such a point.

Computational Details. Different series of cation−π complexes were considered in the study. Initially, we considered the interaction of the Na^+ cation with benzene and its fluoro, hydroxy, amino, boro, chloro, cyano, 1,4-difluoro, and 1,3,5-trifluoro derivatives, as well as pyridine, naphthalene, and indole. The choice of these compounds was motivated by two reasons: (i) they cover a variety of substituents and aromatic cores, which are expected to lead to relevant differences in the π-electron distribution with regard to the benzene molecule and (ii) previous studies have addressed the energetics of the interaction of those compounds with Na^+,[1,12,15] which facilitates examination of the relationship of the electron density topological properties with both energetic and geometrical features in these complexes. Moreover, we extended the study to the interaction of the Na^+ cation with the five-membered rings of azulene, pyrrole, furan, indole, and imidazole. Finally, the interaction of benzene with a variety of cations, including H^+, Mg^{2+}, Li^+, Na^+, and NH_4^+, and hydrogen-bonded neutral molecules, like hydrogen fluoride and methane, was also considered. This allowed us to examine the topological changes in electron density originated from the nature of both the cation and the π-electron system.

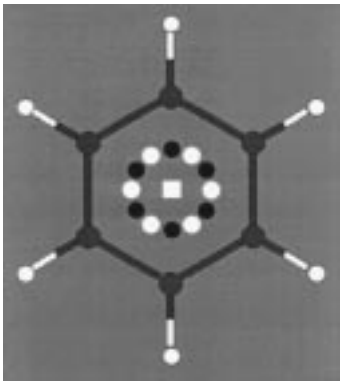

Figure 1. Schematic on-top representation of the location of the six (3, −1) (dark circles) and six (3, +1) (white circles) critical points, and of the (3, +3) (squares) critical point originated from the interaction of the Na^+ cation with benzene. The cation lies in the normal to the benzene passing through the center of the ring.

The geometry of all the complexes was fully optimized at the Hartree−Fock level using the 6-31G(d,p)[30] basis with the only exception of the complex formed between benzene and NH_4^+. In this case the minimum energy structure has two N−H hydrogens directed toward the benzene ring,[8] but we imposed one N−H hydrogen pointing toward the benzene ring in order to allow direct comparison with the rest of the complexes. Interaction energies were determined at the HF/6-31G(d,p) level, since previous studies[1,12,13] demonstrated that reliable quantitative results are obtained at this level of theory, without correction for the basis set superposition error. Indeed, we must note that neither the number nor the quality of the critical points change upon inclusion of electron correlation effects.[31,32]

Results

Table 1 reports the energies and equilibrium distances corresponding to the interaction of Na^+ with a series of benzene derivatives, as well as with pyridine and the six-membered ring of indole and naphthalene. The exploration of the critical points for the interaction of benzene with Na^+ revealed the existence of six (3, −1) critical points, which are symmetrically distributed and connect the cation with the carbon atoms (see Figure 1). The bond path follows closely the geometric line from the carbon atom to the Na^+ ion, since the difference between the bond path length and the interatomic distance is slightly less than 0.01 Å. The Laplacian of the (3, −1) critical points is positive, indicating a depletion of electron energy, as is characteristic of closed-shell interactions.[16,17] There are also six (3, +1) ring critical points, each placed along the line connecting the Na^+ cation with the middle of the C−C bond, that separate every pair of (3, −1) bond critical points (see Figure 1). There is a very small difference between the values of the electron density changes at the alternating bond and ring critical points. Finally, the interaction is further characterized by the existence

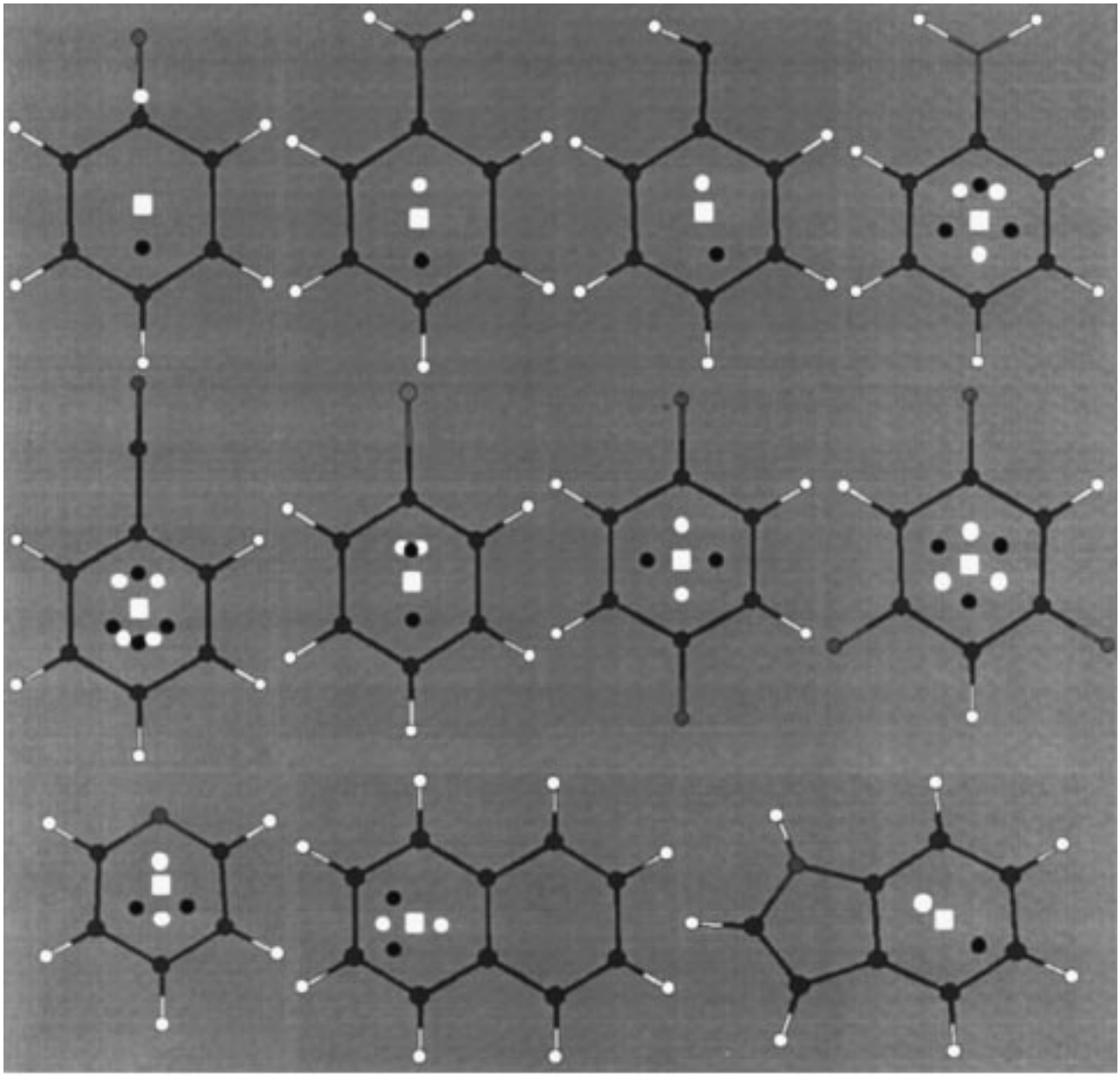

Figure 2. Schematic on-top representation of the location of the (3, −1) (dark circles), (3, +1) (white circles), and (3, +3) (squares) critical points originated from the interaction of the Na^+ cation with benzene derivatives: (top) fluoro, amino, hydroxy, boro; (middle) cyano, chloro, 1,4-difluoro, and 1,3,5-trifluoro; (bottom) pyridine, naphthalene, and the six-membered ring of indole. The cation lies in the normal to the benzene passing through the center of the ring.

of a (3, +3) cage critical point located along the line connecting the Na^+ ion with the center of the ring.

The above-mentioned pattern of critical points that appears upon complexation of the Na^+ ion with benzene is drastically altered by the introduction of substituents (see Table 1 and Figure 2). Only one (3, −1) bond critical point lying between the cation and the carbon at position 4 (para to the substituent) was found for fluorobenzene, aniline, and phenol. The attachment of $-BH_2$ and −CN groups leads to the appearance of three and four bond critical points, respectively. In the former case they connect the cation to carbon atoms C1, C3, and C5, while in the latter the bond path connects the Na^+ ion with atoms C1, C3, C4, and C5. Two bond critical points connecting the cation with atoms C1 and C4 occur in chlorobenzene. Likewise, two and three (3, −1) critical points occur for 1,4-difluoro and 1,3,5-trifluoro derivatives. In the former they are in the plane normal to the molecule passing through the middle of the C2−C3 and C5−C6 bonds, while in the latter they connect the Na^+ ion with the carbon atoms C2, C4, and C6. In the case of pyridine, two bond critical points are found in the line connecting the cation with atoms C3 and C5. Two (3, −1) critical points are found for naphthalene, which connect the cation with carbons C2 and C3. Finally, the approach of Na^+ to the six-membered ring of indole leads to the appearance of one (3, −1) critical point, which connects the cation with C6.

The variation in the number and location of the bond critical points is also reflected in the distribution of the (3, +1) critical points (see Table 1). Thus, the ring critical point in fluorobenzene, aniline, and phenol occurs near the carbon C1, the atom bearing the substituent. A similar pattern is found in chlorobenzene, even though the two symmetrical ring critical points reside very close to the (3, −1) critical point. In the derivatives boro, cyano, 1,4-difluoro, and 1,3,5-trifluoro there is a clear alternance between ring and bond critical points. The two ring critical points in pyridine are in the plane normal to the molecule passing through the line N···C4. Finally, the ring critical point

lies near the bond C9−C10 in naphthalene and the carbon vicinal to the nitrogen in indole.

The topology found in fluorobenzene, aniline, and phenol is particularly interesting. In their complexes a single (3, −1) critical point occurs along the line connecting the carbon C4 and the Na^+ ion (see above) and, in addition to the (3, +1) critical point found in the molecular plane of benzene, a single ring critical point appears near C1. This means that the surface of such a ring critical point extends from the C4−Na^+ bond path all around the ring back to the same bond path and, as a result, the topology of the electron density exhibits a cage critical point in those complexes.

The diversity in the distribution pattern of bond and ring critical points reflects the profound influence of the number and nature of substituents on the electron density of the benzene ring. Thus, the appearance of the bond critical point para to the substituent in fluorobenzene, aniline, and phenol, as well as the ring critical point near the carbon bearing the substituent, reflects the combined influence of the electron-withdrawing and resonance effects of these substituents. Likewise, the pattern found in the mono-, di-, and trifluorinated derivatives can be realized from the electron-withdrawing effect of the fluorine atom. The topological distribution in pyridine can be understood from the deactivating effect of the nitrogen, leading to the bond critical bonds at C3 and C5 and the ring ones near the nitrogen and C4 atoms. Similarly, the location of the bond critical points in naphthalene likely reflects the tendecy to maintain the resonance in the fused six-membered ring, whereas the (3, −1) critical point in indole is formed near the carbon lying in para to the one supporting the nitrogen. Indeed, the influence of the substituent is also noted in the values of the electron density at the bond and ring critical points, which exhibit differences sensibly larger than those found for the benzene−Na^+ complex, revealing more abrupt changes in the electron density distribution (see Table 1). To gain deeper insight into the role of the substituent on the pattern of bond critical points, the Laplacian of the charge density, which determines where the charge density is locally concentrated or depleted, [16,17] and the ellipticities of the phenyl C−H bonds were examined in both the isolated compounds and the complexes. These properties were chosen since they have been used to discuss the directing ability and activating−deactivating effects of a substituent in electrophilic aromatic substitution.[33] Unfortunately, no direct relationship was observed between the bond path distribution and neither the secondary concentration in the valence-shell charge concentration that is found above each of the carbon atoms[33] nor the C−H ellipticities.

The diversity in the topological pattern of the electron density precludes the possibility to relate the energetics of these complexes with the properties of the bond critical points, as has been performed for other intermolecular interactions.[20,23−26] The only common topological feature in all the complexes is the existence of the (3, +3) cage critical point. The values of the density and the Laplacian of the cage critical point, as well as their distance from the ring, are also given in Table 1. Comparison of the energy and equilibrium distances with the properties of the (3, +3) critical points reveals a number of interesting trends. Particularly, there is a strong correlation between the charge density (ρ) at the cage critical point and the interaction energy (E), as noted in the regression equation $E = (59.3-110.4) \times 10^2\rho$ ($r = 0.98$), where the energy is given in kcal/mol and the density is in atomic units (see Figure 3). Furthermore, there is a close correlation between the value of the electron density at the cage critical bond and the equilibrium distance (R_e) from the ring to the Na^+ cation, as shown by the regression equation $R_c = (3.22-0.98) \times 10^2\rho$ ($r = 0.99$), where the equilibrium distance is given in angstroms (see Figure 3). The variation in the location of the cage critical points (r_{cp}) in the complexes follows closely the change in the equilibrium distance ($R_c = 0.99-1.22r_{cp}$; $r = 0.99$; R_e and r_{cp} in angstroms). Finally, there are also strong correlations between the interaction energy ($r = 0.94$) and the equilibrium distance ($r = 0.98$) with the Laplacian of the electron density at the (3, +3) critical point. As noted in previous studies,[26,27,31] these relationships allow us to generalize the concept of bond order to $Na^+-\pi$ interactions.

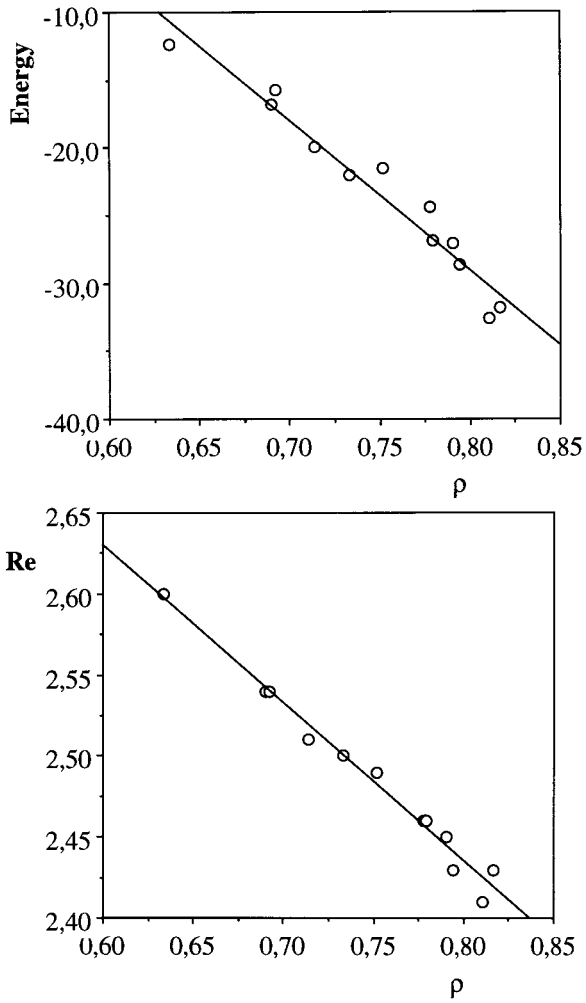

Figure 3. Plots of the regression between the electron density (a.u.) at the (3, +3) critical point and (top) the interaction energy (kcal/mol) and (bottom) the equilibrium distance (Å) for the $Na^+-\pi$ complexes in six-membered rings.

The preceding results point out the relationship between the properties of the cage critical points and the energetics and geometrical characteristics of $Na^+-\pi$ complexes in six-membered rings. This prompted us to investigate the validity of similar relationships in cation−π complexes involving five-membered rings. At this point, we examined the topological features of the electron density for the interaction of Na^+ with pyrrole, imidazole, furan, and the five-membered rings of indole and azulene.

The number and nature of critical points vary considerably between the different molecules (see Table 2 and Figure 4). In the case of pyrrole there are two (3, −1) critical points, which connect the cation with atoms C3 and C4, separated by one ring critical point. Replacement of the carbon C3 of pyrrole by nitrogen (imidazole) leads to the disappearance of one bond

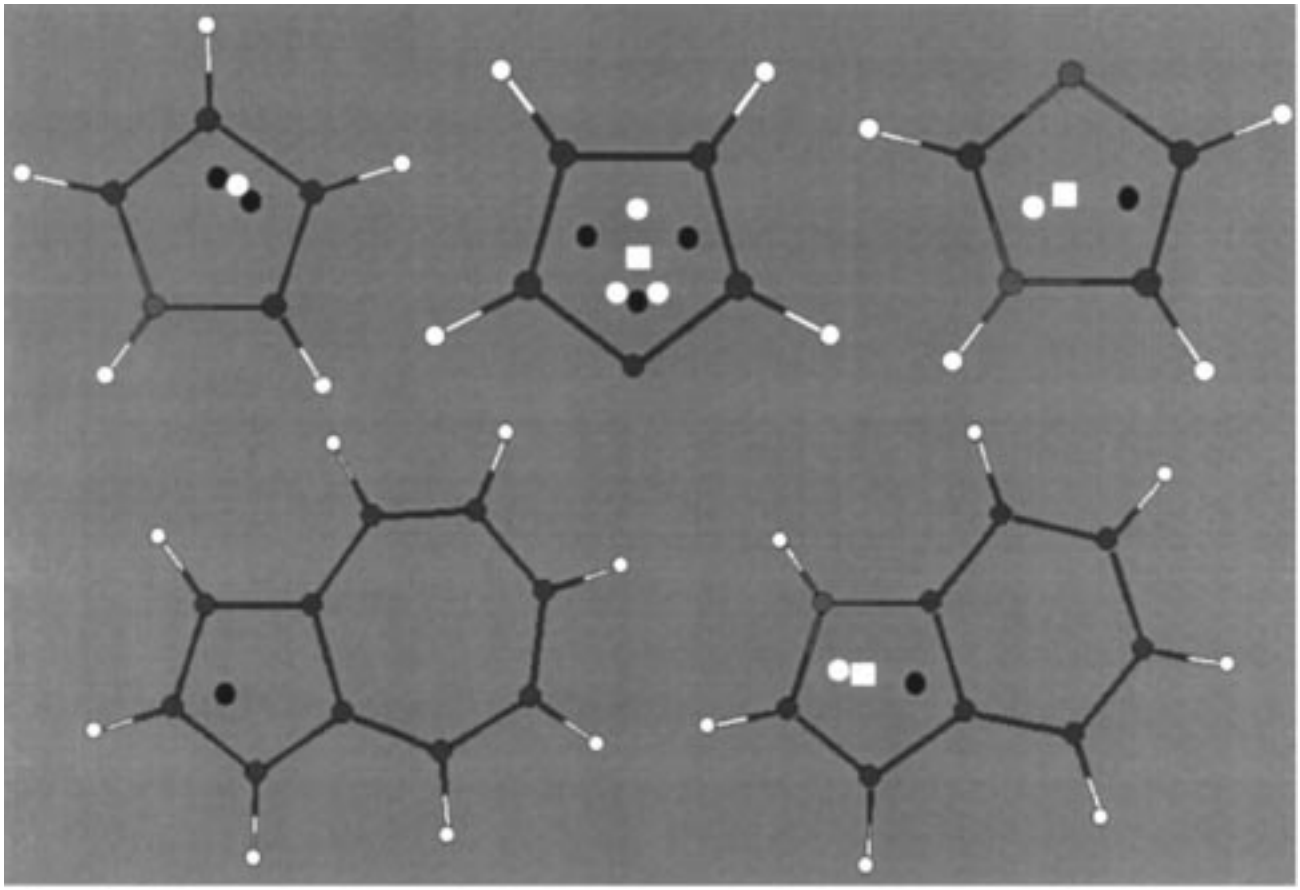

Figure 4. Schematic on-top representation of the location of the (3, −1) (dark circles), (3, +1) (white circles), and (3, +3) (squares) critical points originated from the interaction of the Na^+ cation with (top) pyrrole, furan, and imidazole and (bottom) the five-membered rings of azulene and indole. The cation lies in the normal to the benzene passing through the center of the ring.

TABLE 2: Interaction Energies (*E*, kcal/mol), Equilibrium Distances (R_e, Å), and Selected Electron Density Topological Properties for Na^+−π Complexes Involving Five-membered Rings

compound	E	R_e	CP[a]	n	$10^2\rho$	$10^2\nabla^2\rho$	r_{cp}
azulene	−34.1	2.44	(3, −1)	1	1.379	6.792	1.38
pyrrole	−29.6	2.47	(3, −1)	2	1.341	6.610	1.43
			(3, +1)	1	1.338	6.635	1.42
indole	−29.0	2.47	(3, −1)	1	1.246	6.476	1.42
			(3, +1)	1	0.941	5.684	1.34
			(3, +3)	1	0.928	5.787	1.26
furan	−21.0	2.50	(3, −1)	1	0.919	6.225	1.39
			(3, −1)	2	1.027	5.084	1.47
			(3, +1)	2	0.913	6.100	1.38
			(3, +1)	1	0.946	4.635	1.42
			(3, +3)	1	0.849	5.582	1.29
imidazole	−21.0	2.50	(3, −1)	1	1.123	5.626	1.46
			(3, +1)	1	0.894	5.627	1.40
			(3, +3)	1	0.859	5.692	1.30

[a] The electron density (ρ, atomic units) and its Laplacian ($\nabla^2\rho$, atomic units) at the (3, −1), (3, +1) and (3, +3) critical points (CP) originated upon complexation are given, as well as the total number (n) of each CP in the complex and the distance (r_{cp}, Å) from the aromatic ring to the CP.

critical point, while the bond path of the remaining (3, −1) critical point connects the cation with the atom C4. Likewise, replacement of the NH group of pyrrole by oxygen (furan) leads to three bond critical points, which connect the Na^+ ion with the oxygen and the carbon atoms C2 and C5, each pair of bond critical points being separated by a ring critical point. In the case of indole, a (3, −1) critical point connects the cation with the carbon C4, and there exists a ring critical point opposite to it between the bond N−C2. In azulene there is simply one bond critical point, whose bond path connects the cation with the carbon C10. Finally, in contrast with the topology found for the complexes involving six-membered rings, which all shared a cage critical point, this kind of critical point is found only in furan, imidazole, and indole.

Again, the nature of the heteroatom and of the fused ring largely modulates the topological pattern in complexes involving five-membered rings. Particularly, the large differences arising upon replacement of the NH group in pyrrole by the oxygen atom in furan are remarkable. Thus, whereas the bond critical points appear near C3 and C5 for the former, the reverse trend is observed for furan. This reflects the differences in resonance and electron-withdrawing effects for the groups −NH− and −O−, as noted in the ellipticities of the bond critical points for the bonds N−C2 (pyrrole) and O−C2 (furan) bonds, which amount to 0.110 and 0.019, respectively (0.152 and 0.049 for the uncomplexed molecules). It is also worth noting the effect of the six-membered ring in indole, which makes the bond critical point to appear in the position that reinforces conjugation of the nitrogen lone pair with the fused benzene ring, as compared with the two symmetrical bond critical points in pyrrole. Likewise, the differences observed between indole and azulene suggest that resonance effects are more involved in the former. In fact, it is known that in azulene the bond shared by the two rings, which has the smallest ellipticity (0.074) of all the C−C bonds, is significantly longer than the rest of bonds, indicating a predominantly single-bond character.[32]

The lack of a common topological feature to all the complexes reported in Table 2 precludes establishing relationships similar

TABLE 3: Interaction Energies (*E*, kcal/mol), Equilibrium Distances (R_e, au) and Selected Electron Density Topological Properties for the Complexes of Benzene with Cations and Hydrogen-bonded Neutral Molecules

compound	E	R_e	CP[a]	$10^2\rho$	$10^2\nabla^2\rho$	r_{cp}
H^+	−121.7	1.73	(3, −1)	6.665	7.842	0.63
			(3, +1)	6.663	8.121	0.63
			(3, +3)			
Mg^{2+}	−118.8	3.76	(3, −1)	2.459	10.713	1.18
			(3, +1)	2.451	10.673	1.18
			(3, +3)	1.821	7.048	0.85
Li^+	−40.8	3.67	(3, −1)	1.418	7.673	1.24
			(3, +1)	1.415	7.670	1.24
			(3, +3)	1.161	6.308	1.03
Na^+	−27.1	4.63	(3, −1)	0.991	4.682	1.41
			(3, +1)	0.989	4.671	1.41
			(3, +3)	0.791	4.115	1.19
NH_4^+	−13.9	4.12	(3, −1)	0.973	3.374	1.38
			(3, +1)	0.972	3.377	1.57
			(3, +3)	0.812	3.621	1.16
HF	−3.5	4.72	(3, −1)	0.481	1.981	1.57
			(3, +1)	0.480	1.980	1.57
			(3, +3)	0.433	2.018	1.43
CH_4	−0.3	6.53	(3, −1)	0.122	0.487	2.02
			(3, +1)	0.121	0.487	2.02
			(3, +3)	0.114	0.526	1.92

[a] The electron density (ρ, atomic units) and its Laplacian ($\nabla^2\rho$, atomic units) at the (3, −1), (3, +1) and (3, +3) critical points (CP) originated upon complexation are given, as well as the distance (r_{cp}, Å) from the aromatic ring to the CP.

to those examined before. This behavior is in contrast to the results observed in six-membered rings. In this latter case the effect of changes such as the replacement of −CH− by −N− or the presence of fused rings seems to be better accommodated, as suggested by previous topological studies in azines.[34] In this sense, the electron density in five-membered rings appear to be sensibly more susceptible to the influence of heteroatoms than that in larger rings.

The last point examined here is the characteristics of the cation−π interactions in complexes involving other types of cations or even hydrogen-bonded neutral molecules. Table 3 reports the interaction energies and equilibrium distances for the interaction of benzene with Li^+, Na^+, NH_4^+, and Mg^{2+}, as well as with H^+ and two neutral molecules, hydrogen fluoride and methane, which were also included to examine the interaction with the hydrogen atom in hydrogen-bonded complexes. The topological pattern of critical points reported above for the interaction of benzene with the Na^+ cation is reproduced in all cases (see Figure 1) with the only exception of the interaction with H^+, where no cage critical point was detected. At this point, it must be stressed that no ring critical point was found in the molecular plane of benzene in the benzene−H^+ complex. This is necessary to satisfy the Poincaré−Hopf relationship. In fact, when one examines the profile of the electron density along the line passing through the center of the benzene ring from the H^+, it is found that the electron density decreases monotonically from the maximum value, which occurs at the position of the H^+.

Inspection of the results in Table 3 indicates that, apart from the H^+−benzene complex (see below), there is a relationship between the interaction energy and the electron density at the cage critical point ($E = (25.8-70.0) \times 10^2\rho$; $r = 0.94$). Since all the complexes exhibit the same topological pattern, such an analysis can also be extended to the bond critical points. Thus, there is also a strong correlation between the interaction energy and the electron density at the (3, −1) critical point ($E = (21.9-52.1) \times 10^2\rho$; $r = 0.96$). Moreover, such a correlation is also apparent when one considers the electron density at the (3, −1) critical points located at the C−C bonds (see Table 4), as noted in the regression equation $E = (-3651.1 + 1117.6) \times 10^2\rho$; $r = 0.99$. Similar results are obtained when the Laplacian of the electron density is considered. It is worth stressing the relevance of all these relationships, since they cover a variation of 2 orders of magnitude in the interaction energy and allow for treating simultaneously the interaction with both cations and hydrogen-bonded neutral molecules.

TABLE 4: Electron Density (ρ, Atomic Units) and Its Laplacian ($\nabla^2\rho$, Atomic Units) at the (3, −1) Critical Points Associated with the C−C Bonds in Benzene and Their Ellipticity (ϵ) for the Complexes of Benzene with Cations and Hydrogen-bonded Neutral Molecules[a]

compound	$10^2\rho$	$10^2\nabla^2\rho$	ϵ	q
H^+	3.211	−9.759	0.203	0.57
Mg^{2+}	3.166	−9.575	0.183	1.82
Li^+	3.225	−9.876	0.211	0.94
Na^+	3.236	−9.943	0.215	0.94
NH_4^+	3.251	−10.020	0.224	0.96
HF	3.268	−10.119	0.229	−0.01
CH_4	3.273	−10.161	0.230	0.00

[a] The net charge (q; units of electron) of the interacting compound is also given.

The influence of the interacting (cation or hydrogen-bonded) compound on the electron density can be followed from the ellipticity of the electron density at the (3, −1) critical points of the C−C bonds in the benzene ring. In the case of benzene, the ellipticity of the C−C bond determined from the HF/6-31G-(d,p) wave function is 0.231, which seems reasonable for a bond with an order of 1.5.[35] Table 4 lists the ellipticities determined for the (3, −1) critical points in the C−C bonds. Again, with exception of the H^+−benzene complex, there is a clear relationship between the interaction energy and the electron density deformation induced by the polarizing effect of the interacting molecule ($E = -572.5 + 2500.7\epsilon$; $r = 0.99$).

The preceding results show the generalization of the topological properties of electron density in cation−π complexes to a variety of cations and also to the interaction with the hydrogen atom in hydrogen-bonded neutral molecules. As mentioned above, the only exception to the preceding findings is the interaction of benzene with H^+. The reason for this discrepancy stems from the different nature of the proton, which yields an interaction not defined simply in terms of electrostatic and polarization effects. Thus, very recently,[15] we have shown that the GMIPp (Generalized Molecular Interaction Potential with polarization[36,37]), which evaluates the interaction energy summing up electrostatic, polarization, and van der Waals energy components, reproduces very well the SCF interaction energies for a series of 16 complexes of Na^+ with aromatic compounds. Such an agreement was possible due to the small magnitude of the charge transfer between the aromatic molecule and the cation. In fact, the charge transfer is around 0.05 units of electron for the complexes shown in Table 1 (data not shown) and similar values are found for the complexes given in Table 4. However, the charge transfer in the case of H^+ is on the order of 0.4 units of electron, and accordingly it is expected to contribute decisively to the nature of the interaction with benzene.

Conclusions

The results reported in this study demonstrate the complexity of the topology of the electron density in cation−π complexes, as noted by the variation in the nature and number of critical points. Such a diversity in the topological characteristics reflects

the profound influence exerted by the heteroatoms and substituents on the electron density. Nevertheless, the presence of the cage critical point shared by all the complexes involving six-membered rings allows us to generalize the bond order−bond length relationships reported for other kinds of intermolecular interactions. These relationships are shown to hold for the interaction of Na^+ with a variety of aromatic compounds differing in the substituents and the presence of heteroatoms or fused rings. Indeed, it is also shown that the topological pattern found for the interaction of benzene with Na^+ is applicable to other cations and even to hydrogen-bonded neutral molecules. In contrast, such relationships cannot be established for complexes involving five-membered rings, which likely stems froms a larger difficulty to accommodate the changes in electron density raised by heteroatoms and substituents.

Acknowledgment. We thank Prof. R. W. F. Bader for providing us with a copy of the PROAIM computer program. This work was supported by the DGICYT under projects PB97-0908 and PB96-1005 and by the Centre de Supercomputació de Catalunya (CESCA; Molecular Recognition Project).

References and Notes

(1) Ma, J. C.; Dougherty, D. A. *Chem. Rev.* **1997**, *97*, 1303.
(2) Sussman, J. L.; Harel, M.; Frolow, F.; Oefner, C.; Goldman, A.; Tolker, L.; Silman, I. *Science* **1991**, *253*, 872.
(3) Harel, M.; Scalk, I.; Ehret-Sabatier, L.; Bouet, F.; Goeldner, M.; Hirth, C.; Axelsen, P. H.; Silman, I.; Sussman, J. L. *Proc. Natl. Acad. Sci. U.S.A.* **1993**, *90*, 9031.
(4) Ngola, S.; Dougherty, D. A. *J. Org. Chem.* **1998**, *63*, 4566.
(5) Ting, A. Y.; Shon, I.; Lucero, C.; Schultz, P. G. *J. Am. Chem. Soc.* **1998**, *120*, 7135.
(6) Zoltewicz, J. A.; Maier, N. M.; Fabian, W. M. F. *J. Org. Chem.* **1998**, *63*, 4985.
(7) Deakyne, C. A. In: *Molecular Interactions. From van der Waals to Strongly Bound Complexes*; Scheiner, S., Ed.; Wiley: Chichester, U.K., 1997; pp 265−296.
(8) Kim, K. S.; Lee, J. Y.; Lee, S. J.; Ha, T.-K.; Kim, D. H. *J. Am. Chem. Soc.* **1994**, *116*, 7399.
(9) Lee, J. Y.; Lee, S. J.; Choi, H. S.; Cho, S. J.; Kim, K. S.; Ha, T.-K. *Chem. Phys. Lett.* **1995**, *232*, 67.
(10) Caldwell, J. W.; Kollman, P. A. *J. Am. Chem. Soc.* **1995**, *117*, 4177
(11) Basch, H.; Stevens, W. J. *J. Mol. Struct. (THEOCHEM).* **1995**, *338*, 303.
(12) Dougherty, D. A. *Science* **1996**, *271*, 163.
(13) Mecozzi, S.; West, A. P., Jr.; Dougherty, D. A. *J. Am. Chem. Soc.* **1996**, *118*, 2307.
(14) Chipot, C.; Maigret, B.; Pearlman, D. A.; Kollman, P. A. *J. Am. Chem. Soc.* **1996**, *118*, 2998.
(15) Cubero, E.; Luque, F. J.; Orozco, M. *Proc. Natl. Acad. Sci. U.S.A.* **1998**, *95*, 5976.
(16) Bader, R. F. W. *Chem. Rev.* **1991**, *91*, 893.
(17) Bader, R. F. W. *Atoms in Molecules. A Quantum Theory*; Oxford University Press: Oxford, U.K., 1990.
(18) Carroll, M. T.; Chang, C.; Bader, R. F. W. *Mol. Phys.* **1988**, *63*, 387.
(19) Tang, T.-H.; Hu, W. J.; Yan, D. Y.; Cui, Y. P. *J. Mol. Struct. (THEOCHEM)* **1990**, *207*, 319.
(20) Koch, U.; Popelier, P. *J. Phys. Chem.* **1995**, *99*, 9747.
(21) Gonzalez, L.; Mó, O.; Yañez, M.; Elguero, J. *J. Mol. Struct. (THEOCHEM)* **1996**, *371*, 1.
(22) Alkorta, I.; Rozas, I.; Elguero, J. *Theor. Chim. Acc.* **1998**, *99*, 116.
(23) Popelier, P. L. A. *J. Phys. Chem. A* **1998**, *102*, 1873.
(24) Luque, F. J.; Lopez, J. M.; de la Paz, M. L.; Vicent, C.; Orozco, M. *J. Phys. Chem. A* **1998**, *102*, 6690.
(25) Novoa, J. J.; Lafuente, P.; Mota, F. *Chem. Phys. Lett.* **1998**, *290*, 519.
(26) Boyd, R. J.; Choi., S. C. *Chem. Phys. Lett.* **1985**, *120*, 80.
(27) Boyd, R. J.; Choi., S. C. *Chem. Phys. Lett.* **1986**, *129*, 62.
(28) Alcamí, M.; Mó, O.; Yáñez, M. *J. Phys. Chem.* **1989**, *93*, 3929.
(29) Alcamí, M.; Mó, O.; de Paz, J. L. G.; Yáñez, M. *Theor. Chim. Acta* **1990**, *77*, 1.
(30) Hariharan, P. C.; Pople, J. A. *Theor. Chim. Acta* **1973**, *28*, 213.
(31) Bader, R. F. W.; Tang, T. H.; Tal, Y.; Biegler-König, F. W. *J. Am. Chem. Soc.* **1982**, *104*, 946.
(32) Hanson, A. W. *Acta Crystallogr.* **1965**, *19*, 19.
(33) Bader, R. F. W.; Chang, C. *J. Phys. Chem.* **1989**, *93*, 2946.
(34) Wiberg, K. B.; Nakaji, D.; Breneman, C. M. *J. Am. Chem. Soc.* **1989**, *111*, 4178.
(35) Bader, R. F. W.; Slee, T. S.; Cremer, D.; Kraka, E. *J. Am. Chem. Soc.* **1983**, *105*, 5061.
(36) Orozco, M.; Luque, F. J. In: *Molecular Electrostatic Potentials: Concepts and Applications*; Murray, J., Sen, K., Eds.; Elsevier: Amsterdam, Netherlands, 1996; Vol. 3, pp 181−218.
(37) Luque, F. J.; Orozco, M. *J. Comput. Chem.* **1998**, *19*, 866.

(Esta página está intencionadamente en blanco)

4.2 Interacciones por puente de hidrógeno impropio[1,7]

Los puentes de hidrógeno clásicos, conocidos desde hace más de 50 años, son interacciones no covalentes relativamente fuertes, que presentan propiedades interesantes como la cooperatividad y la direccionalidad. Tienen un papel fundamental en la estructura, las propiedades y la función de las moléculas biológicas y su importancia es enorme en el reconocimiento molecular. Ellos son responsables de muchos modelos de unión entre moléculas, como el apareamiento de las nucleobases en el ADN.

Los puentes de hidrógeno generalmente implican una interacción X-H···Y, donde X y Y son heteroátomos -normalmente nitrógeno, oxigeno o flúor-, uno de ellos se encuentra unido a un átomo de hidrógeno y el otro dispone de pares libres. En los últimos años han aparecido nuevos tipos de puentes de hidrógeno[8,9], es decir, el concepto de puente de hidrógeno se ha extendido a otros complejos. Entre estos inusuales puentes de hidrógeno se incluyen dadores/aceptores de puente de hidrógeno no convencionales, como C-H , distribuciones de carga tipo π o tipo σ, puentes de dihidrógeno, puentes de barrera baja, etc.

Recientemente, se ha identificado un nuevo tipo de puente de hidrógeno impropio o *blue shifting*[7], denominado originalmente *anti-hydrogen bond*, que se caracteriza por un acortamiento del enlace C-H y un desplazamiento hacia la zona azul de la frecuencia de vibración de este enlace. Esto contrasta con los puentes de hidrógeno convencionales, que están caracterizados fenomenológicamente por un alargamiento del enlace X-H y un desplazamiento de la frecuencia vibracional del enlace hacia el rojo. Los sistemas que poseen este tipo de interacciones tienen el siguiente esquema: C-H···π, C-H···O, C-H···F y C-H···X^- (X= halogeno).

El hecho que sistemas con uniones C-H···O presenten este tipo de comportamiento nos conduce a la posibilidad que las bases nitrogenadas de los ácidos nucleicos interaccionen entre ellas a través de este nuevo tipo de puentes de hidrógeno.

Para ello, primero se estudia la naturaleza de este tipo de interacciones en sistemas modelo y más adelante se amplía este estudio a las interacciones entre pares de bases presentes en los ácidos nucleicos.

En el apartado 4.2.1 se muestra un análisis comparativo de las propiedades topológicas de la densidad electrónica de una serie de complejos C-H···π, que presentan puentes de hidrógeno normales y puentes de hidrógeno impropios. La teoría AIM[6] ofrece la posibilidad de examinar la naturaleza de este tipo de interacciones.

En el apartado 4.2.2 se determina la naturaleza de los puentes de hidrógeno que se establecen entre los pares A·U WC, U·U 7 y U·U C, utilizando el mismo tipo de análisis del punto anterior, la teoría AIM[6].

Los cálculos geométricos, energéticos y vibracionales de estos pares de bases, junto con el análisis NBO[10] (*Natural bond orbital*) han sido realizados por los Profs. P. Hobza y J. Šponer.

4.2.1 Hydrogen bond versus anti-hydrogen bond: A comparative analysis based on the electron density topology

Elena Cubero, Modesto Orozco, Pavel Hobza & F. Javier Luque

J. Phys. Chem. A. **1999**, *103*, 6394-6401

(Esta página está intencionadamente en blanco)

Hydrogen Bond versus Anti-Hydrogen Bond: A Comparative Analysis Based on the Electron Density Topology

E. Cubero,[†] M. Orozco,*[,†] P. Hobza,[‡] and F. J. Luque*[,§]

Departament de Bioquímica i Biologia Molecular, Facultat de Química, Universitat de Barcelona, Martí i Franqués 1, 08028 Barcelona, Spain, J. Heyrovsky Institute of Physical Chemistry, Academy of Sciences of the Czech Republic, 182 23 Prague 8, Czech Republic, and Departament de Fisicoquímica, Facultat de Farmàcia, Universitat de Barcelona, Av. Diagonal s/n, 08028 Barcelona, Spain

Received: January 22, 1999; In Final Form: April 14, 1999

The theory of atoms in molecules is used to examine the nature of anti-hydrogen bond (anti-H bond) interaction. Contrary to what is found in normal hydrogen bond (H bond) complexes, which are characterized by lengthening of the X−H bond and a red shift of its stretching frequency, the anti-H bond leads to a shortening of the X−H bond length and a blue shift of its vibrational frequency. The topological properties of the electron density have been determined for a series of C−H···π complexes, which exhibit either anti-H bond or normal H bond character, as well as for the complexes C_6H_5F···$HCCl_3$ and C_6H_6···HF, which are representative cases of anti- and normal H bonds. Inspection of the set of topological criteria utilized to characterize conventional H bonds shows no relevant difference in the two classes of H···π complexes. Analysis of the results suggests that the specific features of the anti-H bond originates from the redistribution of electron density in the C−H bond induced upon complexation, which in turn evidences the different response − dispersion versus electrostatic− of the interacting monomer for stabilizing the complex.

Introduction

The hydrogen bond (H bond) is a key interaction in molecular recognition.[1,2] From an energetic point of view, a H bond typically contributes a few kilocalories per mole to the stabilization of H-bonded complexes, even though it can be as large as −50 kcal/mol in complexes such as $(FHF)^-$.[3] The H bond presents an interesting set of properties such as cooperativity and directionality, which are relevant for determining a wide range of structural properties, like the aggregation states of water[4] and the stability of biomolecules.[5] Indeed, the distribution of H bond donors and acceptors has a functional role in modulating the specificity of recognition and binding in chemical and biological systems.[2] This feature has been exploited, for instance, to design new agents in the context of antigen and antisense therapies.[6]

Conventional H bond interactions (X−H···Y) involve two electron-withdrawing atoms (X,Y are usually nitrogen, oxygen, or fluorine), one being attached to a hydrogen atom and the other bearing lone electron pairs. These complexes are characterized by a lengthening of the donor X−H bond and by a concomitant red shift in the X−H stretching frequency. Nevertheless, recent studies have shown that such a concept of hydrogen bonding is not complete and can be extended to other complexes, like those involving the interactions with π charge distributions (Y: π-electron system)[7] or with carbon atoms acting as hydrogen donors (X: carbon).[8] Indeed, a new type of H bond, called a dihydrogen bond, has been introduced to explain certain interactions where a hydrogen is directly donated to another hydrogen (X−H···H−Y), the latter being negatively charged.[9] These interactions have been described in systems containing transition metals and boron, which can accommodate the hydridic hydrogen.[10]

Recently, Hobza et al.[11] have suggested the existence of a new type of bonding, termed anti-hydrogen bond (anti-H bond), which has been identified in the T-shape structure of the benzene dimer and other benzene complexes interacting with carbon proton donors. In contrast to the features observed in conventional H bonds, the anti-H bond is characterized by a shortening of the C−H bond and by a blue shift of the C−H stretching frequency. Stabilization in these complexes originates dominantly in the London dispersion energy and no (or very small) stabilization is found at the Hartree−Fock level.[11] Dispersion attraction is proportional to the higher power of the reciprocal distance of the centers of mass of both subsystems. To minimize the distance and thus optimize the dispersion attraction, it is advantageous to compress the C−H bond of the proton donor. Forces causing shortening of the C−H bond are responsible for making the C−H stretching potential deeper and narrower, and thus allow for a blue shift of the corresponding stretching frequency. Recently, the predicted anti-H bond nature of the complex between chloroform and fluorobenzene has been confirmed experimentally.[12]

To gain insight into the nature of anti-H bond, this study reports a comparative analysis of the electron density topology in complexes corresponding to normal H bonds and anti-H bonds for a series of C−H···π complexes. The theory of "atoms in molecules" (AIM)[13] offers a rigorous way of partitioning any system into its atomic fragments considering the gradient vector field of its electron density. By means of a topological analysis of the electron density, features such as bond critical points and paths of maximum electron density can be utilized to draw a

* To whom correspondence should be sent.
[†] Departament de Bioquímica i Biologia Molecular.
[‡] J. Heyrovsky Institute of Physical Chemistry.
[§] Departament de Fisicoquímica.

10.1021/jp990258f CCC: $18.00 © 1999 American Chemical Society
Published on Web 07/27/1999

TABLE 1: Length (bl; Å) and Harmonic Stretching Frequency (ν; cm^{-1}) of the C−H Bond in the Isolated Monomer (m) and in the Dimer (d), and the Interaction Energy (kcal/mol) of the Complex

compound	bl(m)	bl(d)	Δbl	ν(m)	ν(d)	Δν	ΔE^a
CH_4	1.0855	1.0846	−0.0009	3278	3293	+15	−0.4 (−1.5)
$HCCl_3$	1.0829	1.0806	−0.0023	3256	3307	+51	−3.2 (−6.5)
C_6H_6	1.0827	1.0793	−0.0034	3283	3325	+42	−1.2 (−3.5)
HCCH	1.0625	1.0633	0.0008	3588	3586	−2	−1.6 (−3.7)
HCN	1.0652	1.0667	0.0015	3531	3515	−16	−3.2 (−5.4)
HF	0.9211	0.9239	0.0028	4194	4153	−41	−2.8 (−5.3)
$HCCl_3$[b]	1.0829	1.0802	−0.0027	3256	3309	+53	−2.5 (−5.8)

[a] The interaction energy estimated without correction for the basis set superposition error and geometry distortion of the monomers upon complexation is given in parentheses. [b] Complex of chloroform with fluorobenzene.

molecular graph (i.e., the network of bond paths that connects linked atoms). In particular, an H bond is evidenced in the charge density by a bond path linking the proton and the acceptor atom. AIM has been successfully used to characterize H bonds in a variety of molecular complexes.[7a,7e,8c,9b,14] Several studies have also shown a clear relationship between the topological properties of the charge density in H-bonded complexes with both the interaction energy and the internuclear distance of the complexes.[7e,15] Therefore, AIM seems well suited to examine the very nature of the anti-H bond in molecular clusters.

Methods

To examine the electron density topological properties in H bonds and anti-H bonds, the benzene complexes with CH_4, $CHCl_3$, C_6H_6, and HCN were considered. These complexes were chosen following Hobza et al.,[11] who used them to discuss the C−H···π anti-H bonds for the proton donors CH_4, $CHCl_3$, and C_6H_6, which exhibited changes (shortening of the C−H bond and blue shift in the stretching frequency) opposite to those expected for a normal H bond, as was found in the complex of benzene with HCN (lengthening of the C−H bond and red shift in the stretching frequency). In addition, we considered the interaction of benzene with HCCH and HF. Because HCCH can be viewed as an apolar isoster of HCN, inspection of the topological properties can be of interest for a comparative analysis. On the other hand, inclusion of the complex between benzene and HF is useful as a reference model because this complex is expected to behave as a prototypical normal H bond. Finally, the analysis was extended to the H bond interaction in the complex of chloroform with fluorobenzene because the blue shift in the C−H stretching frequency predicted by theory has been confirmed experimentally.[12]

The geometries of complexes and isolated monomers were optimized at the second-order Møller−Plesset level[16] using the 6-31G(d,p)[17] basis set and the frozen core approximation. No symmetry constraint was imposed in the optimization. In the starting geometry, the complexes were built up with the donor C−H group oriented along the line normal to the plane of benzene passing through the center of the ring. For the complex of chloroform with fluorobenzene, we used as starting geometry the MP2/6-31G(d) optimized one reported by Hobza in ref 12. The minimum energy nature of the optimized structures was verified from vibrational frequency analysis. With exception of the benzene complexes with methane and hydrogen fluoride, the optimized geometries present the donor C−H group pointing toward the center of the benzene ring. In the C_6H_6···HCH_3 and C_6H_6···HF complexes, the C−H and F−H bonds are pointing toward a carbon atom of the ring, and the optimized geometry has a C_s symmetry. To compare the topological properties of the electron density, additional energy minimization calculations were performed for these two complexes imposing the C−H and F−H bonds to be oriented along the normal line passing through the center of the benzene ring. Even though the final structures presented nonzero negative frequencies, they were used in the analysis because they exhibit a common topological pattern with the other benzene complexes (vide infra). However, comparison is also made of the topological properties of the C_s-optimized structures. The interaction energies were corrected for the basis set superposition error using the counterpoise correction.[18] The C−H stretching frequency shifts induced upon complexation were determined within the harmonic approximation because the introduction of anharmonicity does not substantially modify the results.[11] All these calculations were performed with Gaussian 94.[19] The topological analysis and the integration of selected atomic properties (vide infra) was performed with the programs EXTREME and PROAIM.[20]

Results and Discussion

Table 1 reports the lengths and harmonic stretching frequencies of the C−H bond in the monomer and the dimer, and the interaction energy of the dimer, for the benzene complexes with CH_4, $CHCl_3$, C_6H_6, HCN, HCCH, and HF, as well as of chloroform with fluorobenzene. In all cases, the C−H (F−H) bond is pointing toward the center of the ring. Upon complexation, the C−H bond length decreases for CH_4 (−0.0010 Å), $CHCl_3$ (−0.0023 Å; −0.0027 Å for the complex with fluorobenzene), and C_6H_6 (−0.0034 Å),[11] whereas the reverse effect occurs in HCN (+0.0153 Å) and HCCH (+0.0008 Å). This latter trend is also found in the complex with HF, where the H−F bond length increases 0.0028 Å. The lengthening/shortening of the C−H bond upon complexation is also reflected in the change of the corresponding stretching frequency. Thus, whereas benzene complexation leads to a blue shift in the range +15 to +51 cm^{-1} for CH_4, $CHCl_3$, and C_6H_6, the C−H frequency is red shifted very slightly in HCCH (−2 cm^{-1}) and more remarkably in HCN (−16 cm^{-1}), as it is also found in the complex with HF, where the H−F stretching frequency is red shifted by 41 cm^{-1}. In summary, in contrast to the behavior exhibited by conventional complexes, such as C_6H_6···HCN and C_6H_6···HF, the reverse features found for other complexes provides the basis for the concept of the anti-H bond.[11]

In the true minimum energy structures of the complexes of benzene with methane and hydrogen fluoride (see *Methods*) the C−H and F−H bonds are pointing toward a carbon atom of the ring (the C−H or F−H axis forms an angle of ∼15° with the line normal to the benzene passing through the center of the ring). The optimized geometry for C_6H_6···HF differs from the minimum energy structures reported in previous studies, where a C_{6v} symmetry was found at the RHF/6-31G(d) level,[7a] and where the HF molecule points toward the middle point of one of the C−C bonds at the MP2/6-311++G(d,p) level.[14c] The energy of the MP2/6-31G(d,p) C_s structures differ only by a few hundredths of a kilocalorie/mole from the values reported

in Table 1, indicating that the energy surface is very flat and that the energy minimum is very shallow. For the purposes of our study, it is worth noting that in the C_s structures the C−H bond of methane is shortened by 0.0008 Å and the C−H stretching frequency is blue shifted by 13 cm^{-1}, whereas in contrast the H−F bond length is enlarged 0.0034 Å and a red shift of −59 cm^{-1} occurs in the vibrational frequency. Therefore, despite the different geometrical arrangement, the changes in bond length and stretching frequency observed in CH_4 and HF reflect the same differential trends already mentioned.

As noted before by Hobza et al.,[11] the stabilization in anti-H bond complexes originates dominantly in the London dispersion energy. Thus, decomposition of the interaction energies reported in Table 1 into their Hartree−Fock and MP2 components indicate that the former term is repulsive, varying from +0.7 kcal/mol for the complex of benzene with chloroform to +1.9 kcal/mol for that with benzene. In contrast, the Hartree−Fock component is stabilizing for the complexes of benzene with HCN and HF, where it contributes to around −1.9 kcal/mol to the total interaction energy.

In a series of studies, Popelier proposed a set of eight concerted effects occurring in the electron density that are indicative of hydrogen bonding.[8c,9b] These criteria comprise a set of local topological properties of the electron density and a set of integrated atomic properties related to the hydrogen atom involved in hydrogen bonding. With regard to the former set, the existence of a H bond implies (1) a correct topological pattern (a bond critical point and a bond path) for the proton donor and acceptor, proper values of (2) the electron density and (3) the laplacian of the electron density at the bond critical point, and finally (4) the mutual penetration of the hydrogen and acceptor atoms. The criteria concerning the integrated properties of the hydrogen atom involve (5) an increase of the net charge, (6) an energetic destabilization, (7) a decrease in the dipolar polarization, and finally (8) a decrease in the atomic volume. These properties have been determined for the different complexes considered in this study and are used to compare the AIM features in normal H bond and anti-H bonds.

(1) Topology of the Electron Density. The first necessary condition for the existence of an H bond is the identification of a (3,−1) bond critical point between the hydrogen atom and the acceptor associated with a bond path linking the corresponding atoms. In the C−H···benzene complexes considered here, the acceptor is the set of attractors formed by the carbon atoms in the benzene ring, and the formation of the H bond is reflected in the appearance of six (3,−1) critical points linking the hydrogen atom to each carbon atom[7a,e] (see Figure 1). In addition, a common feature to all the complexes is the occurrence of six (3,+1) ring critical points, which are placed between each pair of bond critical points. Finally, the C−H···π interaction is also characterized by the formation of a (3,+3) cage critical point. This topological pattern has also been described in complexes involving the interaction of cations with benzene.[7e]

The complex between chloroform and fluorobenzene is peculiar because just one bond critical bond exists, and the corresponding bond path connects the hydrogen atom in chloroform with the carbon in position *para* of fluorobenzene (see Figure 1). Indeed, the interaction is characterized by the appearance of a ring critical point near C1 and by a cage critical point over the center of the ring. It is worth noting that such topology satisfies the Poincaré−Hopf relationship, which relates the number and type of critical points that can coexist in a system with a finite number of nuclei. This topological

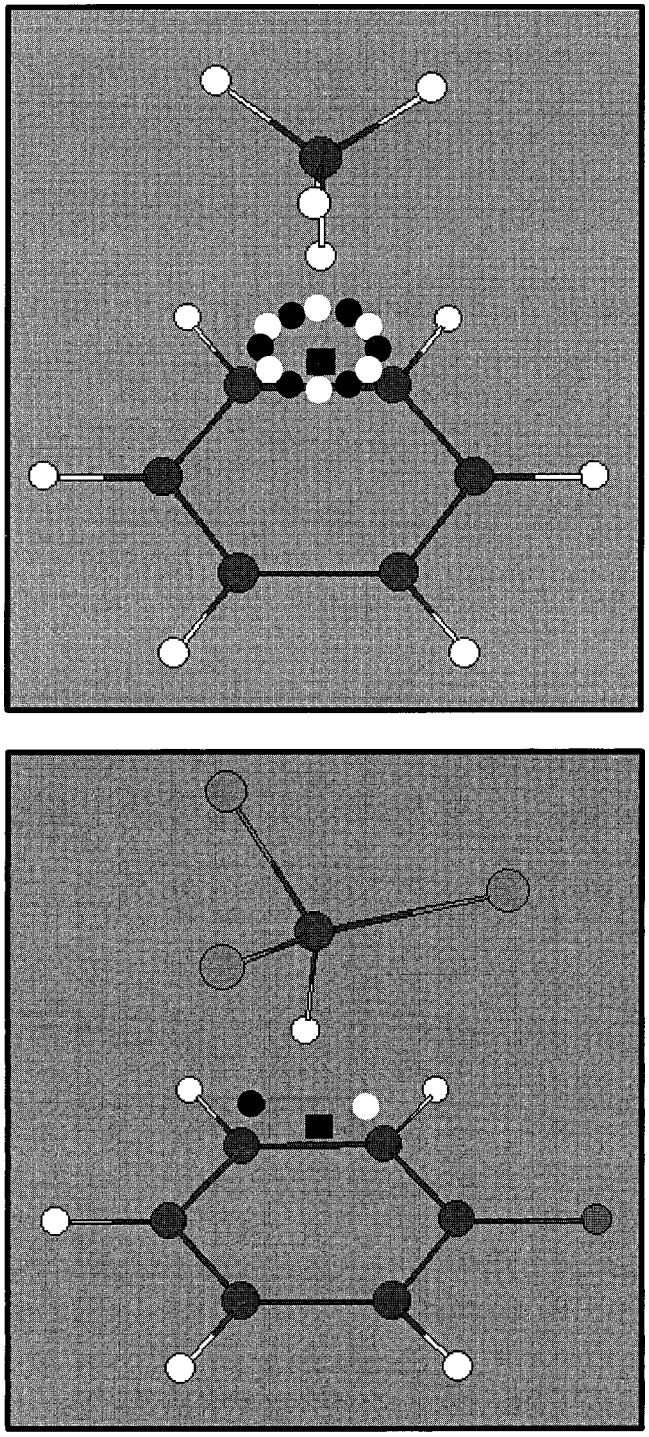

Figure 1. Representation of the dimer between benzene and methane (top) and fluorobenzene and chloroform (bottom) showing the location of the bond (dark circles), ring (white circles), and cage (square) critical points formed upon complexation.

arrangement has also been found in the complex of fluorobenzene with the Na^+ cation[7e] and reflects the influence of the fluorine atom on the electron density of the benzene ring. It suggests that the surface of the ring critical point extends from the C(*para*)-H bond path all around the ring back to the same bond path and, as a result, the topology of the electron density exhibits a cage critical point in the complex.[21]

The C_s structures for the benzene complexes with CH_4 and HF also exhibit a different pattern. In these cases, a single bond path links the hydrogen atom with the carbon atom to which the C−H (F−H) bond is pointing. In addition, a ring critical

TABLE 2: Topological Properties (au) of the Electron Density at the Bond, Ring, and Cage Critical Points (CP) Originated upon Formation of the C−H···π Complexes

compound	CP	ρ	$\nabla^2\rho$	λ_1	λ_2	λ_3
CH_4	(3,−1)	0.0049	0.0169	−0.0028	−0.0001	0.0197
	(3,+1)	0.0048	0.0169	−0.0028	0.0001	0.0196
	(3,+3)	0.0043	0.0180	0.0028	0.0028	0.0125
$HCCl_3$	(3,−1)	0.0102	0.0357	−0.0075	−0.0004	0.0435
	(3,+1)	0.0101	0.0358	−0.0075	0.0004	0.0429
	(3,+3)	0.0084	0.0383	0.0090	0.0090	0.0202
C_6H_6	(3,−1)	0.0077	0.0271	−0.0051	−0.0002	0.0325
	(3,+1)	0.0077	0.0272	−0.0052	0.0002	0.0321
	(3,+3)	0.0065	0.0290	0.0059	0.0059	0.0172
HCCH	(3,−1)	0.0075	0.0266	−0.0050	−0.0002	0.0138
	(3,+1)	0.0074	0.0265	−0.0049	0.0002	0.0312
	(3,+3)	0.0064	0.0281	0.0055	0.0055	0.0171
HCN	(3,−1)	0.0086	0.0302	−0.0059	−0.0003	0.0363
	(3,+1)	0.0085	0.0302	−0.0059	0.0002	0.0359
	(3,+3)	0.0072	0.0320	0.0067	0.0067	0.0185
HF	(3,−1)	0.0083	0.0319	−0.0059	−0.0002	0.0381
	(3,+1)	0.0083	0.0319	−0.0059	0.0002	0.0377
	(3,+3)	0.0072	0.0321	0.0063	0.0063	0.0194
$HCCl_3$[a]	(3,−1)	0.0108	0.0365	−0.0088	−0.0016	0.0470
	(3,+1)	0.0089	0.0341	−0.0061	0.0011	0.0391
	(3,+3)	0.0078	0.0379	0.0085	0.0092	0.0202

[a] Complex of chloroform with fluorobenzene.

point and a cage critical point are also found for the complex of benzene with methane, they exhibit an arrangement similar to that found for the complex of chloroform with fluorobenzene. Again, these topologies satisfy the Poincaré−Hopf relationship. Thus, even though the energy difference between the C_s geometries and those having the C−H (F−H) group pointing toward the center of the ring is very small (vide supra), marked changes occur in the topology of the electron density.

(2) Charge Density at the Bond Critical Point. According to previous studies, the electron density at the bond critical point formed in hydrogen bonding varies typically in the range 0.002−0.034 atomic units (au), these values being sensibly lower than those found for (3,−1) critical points associated with covalent bonds. Table 2 reports the values of the electron density at the (3,−1), (3,+1), and (3,+3) critical points formed upon complexation with benzene.[22] The electron density at the bond critical points, which varies from ∼0.004 au in CH_4 to near 0.011 au in $CHCl_3$, fits within the expected range of values for similar interactions.[8c,9b]

Comparison of the density values at the (3,−1) critical points given in Table 2 with the corresponding interaction energies of the benzene complexes (Table 1) shows the existence a linear relationship (see Figure 2), as noted in the correlation coefficient ($r = 0.91$) of the regression equation $E = 2.716 - 6.036\ 10^2\rho$ (the energy is given in kcal/mol and the density in au). Analogous findings have been observed between the density at the (3,−1) critical point and the interaction energy in a variety of complexes.[15] Because all the complexes exhibit the same topological pattern, such a comparison can be performed considering the density at the (3,+1) and (3,+3) critical points. In particular, the following relationship holds for the density at the cage critical points: $E = 3.165 - 7.797\ 10^2\rho$ ($r = 0.92$), which agrees with similar findings recently reported for cation-π complexes.[7e] These relationships allow us to generalize the concept of bond order reported for other kinds of related interactions.[15]

(3) Laplacian of the Charge Density. It has been shown that the value of $\nabla^2\rho$ for the (3,−1) critical point in H bonds, and more generally for closed-shell interactions such as ionic bonds and van der Waals complexes, is positive. This feature is found

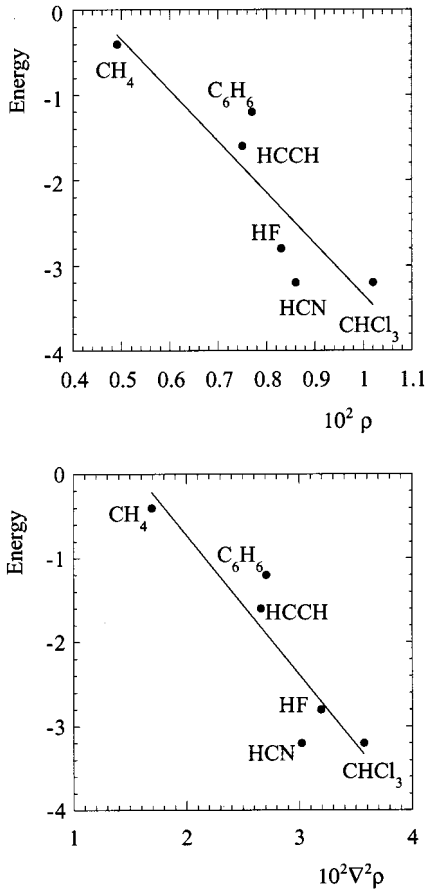

Figure 2. Representation of the variation in the BSSE-corrected interaction energy (kcal/mol) of the C−H···benzene complexes and the electron density (top) at the bond critical point and its laplacian (bottom).

in all the complexes (Table 2) and the values for the bond critical points, which are between 0.016 and 0.037 au, are similar to the range of values for typical H-bonded interactions, which can vary from 0.014 to 0.139 au.[8c] The positive value of the laplacian indicates a depletion of electron density from the interatomic surface toward the interacting nuclei, as noted in the positive value of λ_3, which is much larger than the other two eigenvalues. Another feature of the laplacian is the large magnitude of the ellipticity, which is defined as $\lambda_1/\lambda_2 - 1$, because it can be as large as 40 for the (3,−1) critical point formed upon complexation. This feature is an indication of structural instability, as it is also revealed by the closeness between bond and ring critical points.

Following the trends just mentioned for the electron density at the bond critical point, there is a clear relationship between the BSSE (basis set superposition error)-corrected interaction energy of the benzene complexes and the laplacian of the electron density, as can be stated from inspection of Figure 2. The regression equations for the bond and cage critical points are $E = 2.649 - 1.668\ 10^2\nabla^2\rho$ ($r = 0.92$) and $E = 2.608 - 1.569\ 10^2\nabla^2\rho$ ($r = 0.92$), respectively.

(4) Mutual Penetration of Hydrogen and Acceptor Atoms. The mutual penetration can be determined by comparison of the nonbonded radii (r^0) of both hydrogen and acceptor atoms with the corresponding bonded radii (r). The nonbonded radius was estimated as the distance from the nucleus to a given charge density contour (usually taken to be 0.001 au) in the direction of the H bond, whereas the bonded radius is determined from the distance of the nucleus to the bond critical point formed

TABLE 3: Nonbonded (r^0) and Bonded (r) Radii (au) of the Hydrogen and Carbon Atom for the Series of Benzene Complexes

compound	r^0_H	r_H	Δr_H [a]	r^0_C	r_C	Δr_C [a]	$\Delta r_H + \Delta r_C$
CH_4	2.59	2.24	0.35	3.95	3.41	0.54	0.89
$HCCl_3$	2.52	1.89	0.63	4.02	3.00	1.02	1.65
C_6H_6	2.58	2.04	0.54	3.97	3.14	0.83	1.37
HCCH	2.44	1.97	0.47	4.00	3.18	0.82	1.29
HCN	2.40	1.89	0.51	4.00	3.10	0.90	1.41
HF	2.12	1.73	0.39	4.03	3.11	0.92	1.31
$HCCl_3$ [b]	2.52	1.86	0.66	3.98	2.97	1.01	1.67

[a] $r^0 - r$. [b] Complex of chloroform with fluorobenzene.

TABLE 4: Integrated Atomic Properties[a] of the H Bond Hydrogen Atom in the Isolated Monomer and In the Complex, and the Change (Δ) of the Corresponding Property Arising Upon Complexation

compound	monomer	complex	Δ
	net charge		
CH_4	−0.027	−0.003	0.024
$HCCl_3$	0.097	0.128	0.031
C_6H_6	−0.008	0.018	0.026
HCCH	0.125	0.149	0.024
HCN	0.182	0.209	0.027
HF	0.713	0.716	0.003
$HCCl_3$ [b]	0.097	0.133	0.036
	energy		
CH_4	−0.6395	−0.6339	0.0056
$HCCl_3$	−0.6117	−0.6021	0.0096
C_6H_6	−0.6374	−0.6340	0.0034
HCCH	−0.5730	−0.5643	0.0087
HCN	−0.5466	−0.5362	0.0104
HF	−0.2919	−0.2879	0.0040
$HCCl_3$ [b]	−0.6117	−0.5950	0.0167
	first moment		
CH_4	0.134	0.110	−0.024
$HCCl_3$	0.132	0.107	−0.025
C_6H_6	0.128	0.097	−0.031
HCCH	0.114	0.096	−0.018
HCN	0.110	0.094	−0.016
HF	0.120	0.114	−0.006
$HCCl_3$ [b]	0.132	0.094	−0.038
	volume		
CH_4	51.59	48.05	−3.54
$HCCl_3$	41.72	28.97	−12.75
C_6H_6	50.27	40.77	−9.50
HCCH	42.89	36.43	−6.46
HCN	40.16	31.27	−8.89
HF	14.24	9.82	−4.42
$HCCl_3$ [b]	41.72	29.70	−12.02

[a] All values in atomic units. [b] Complex of chloroform with fluorobenzene.

upon complexation. The penetration is then defined as the difference between the nonbonded and bonded radius ($\Delta r = r^0 - r$). Table 3 shows the corresponding results, which indicate that in all cases the penetrations are positive and that the carbon atoms of the benzene ring are more penetrated that the hydrogen atom, in agreement with previous studies for related systems.[14c,d]

(5) Increase of Net Charge of the Hydrogen Atom. Another necessary condition for the formation of a H bond is the loss of charge of the hydrogen atom. The values of the net charge for the hydrogen atom in the isolated monomer and in the dimer, as well as their difference, are shown in Table 4. The results indicate that the hydrogen is descreened upon formation of the complex. The magnitude of this effect is between 0.022 and 0.036 units of electron for all the complexes but the dimer benzene···HF, where the net charge of the hydrogen atom increases only 0.003 units of electron upon binding. This particular behavior can be explained from the large descreening of the hydrogen in the isolated HF that is due to the strong electron-withdrawing nature of the fluorine atom. In all cases, there is a charge transfer from the aromatic ring to the proton donor molecule, which varies from only 0.004 units of electron for CH_4 to ∼0.025 units of electron for the polar molecules $CHCl_3$, HCN, and HF.

(6) Energetic Destabilization of the Hydrogen Atom. Another feature of H bond is the energetic destabilization of the hydrogen atom, which can be determined from the difference in atomic energies of the hydrogen in the isolated monomer and in the dimer. The results reported in Table 4 indicate that this quantity is positive in all cases, ranging from 0.0034 to 0.0104 au, which agrees with the destabilization observed in other H bond interactions.[8c,9b,14c,d]

(7) Decrease of Dipolar Polarization of the Hydrogen Atom. In addition to the preceding integrated properties, the first moment of the hydrogen atom must decrease upon formation of a H bond. The results in Table 4 show that complexation with benzene (and fluorobenzene) leads to a reduction in the first moment, which decreases between 0.006 (HF) and 0.031 ($CHCl_3$) au. Again, this range of variation compares with the changes observed in a variety of H bond complexes.[8c,9b]

(8) Decrease of the Atomic Volume of the Hydrogen Atom. The last criterion for the existence of a H bond is the decrease in the atomic volume of the hydrogen atom. The corresponding values for the isolated monomer and for the dimer are collected in Table 4. Inspection of the results indicate that the volume of the hydrogen atom is reduced by 3−13 au with regard to the volume in the isolated monomer. The change experienced by the hydrogen atom is sensibly larger than the variations observed in the rest of atoms within the molecule (data not shown), leading to a net reduction of the molecular volume in all the cases.

The preceding results indicate that the hydrogen atom involved in H-bonding exhibits analogous topological features of the electron density and similar changes in the integrated atomic properties in all cases. This common pattern consists of the appearance of a bond path linking the hydrogen atom to each carbon atom in the benzene ring and the corresponding bond critical point. The electron density at the (3,−1) critical point and its laplacian, which is positive as expected for a closed-shell interaction, fit within the expected range for H bond interactions. Finally, inspection of the integrated properties reveal a loss of electron density, which is accompanied by a reduction in the atomic volume, an energy destabilization of the atom, and a decrease in the atomic polarization. Therefore, as far as the criteria defining an H bond interaction are concerned, there is no relevant difference in the properties associated with the hydrogen atom for the series of compounds examined here, even though the results in Table 1 indicate that there is a fundamental division between complexes exhibiting features of conventional H bond or anti-H bond behavior. This result suggests that the phenomenon of the anti-H bond stems from the electron density redistribution in the C−H bond induced upon complexation. In an attempt to examine this assumption, we have determined the properties of the (3,−1) critical point associated with the C−H bond in the complex and in the isolated monomers.

Table 5 shows the distance from the bond critical point (BCP) to the carbon and hydrogen nuclei in the isolated monomer and in the complex. The results indicate that, as a result of complexation, the distance from the (3,−1) critical point to the carbon nucleus increases and the separation of the bond critical point to the hydrogen nucleus decreases. The magnitude of the

TABLE 5: Distance (au) of the (3,−1) Bond Critical Point (BCP) Associated with the C−H Bond to the Carbon and Hydrogen Nuclei in the Isolated Monomer and in the Complex

	BCP−carbon			BCP−hydrogen			
compound	m	d	Δ^a	m	d	Δ^a	net effect
CH_4	1.2735	1.2825	0.0090	0.7779	0.7670	−0.0109	−0.0019
$HCCl_3$	1.3418	1.3599	0.0181	0.7045	0.6822	−0.0283	−0.0042
C_6H_6	1.2783	1.2884	0.0101	0.7678	0.7512	−0.0166	−0.0065
HCCH	1.2927	1.3108	0.0181	0.7150	0.6985	−0.0165	0.0016
HCN	1.3206	1.3426	0.0220	0.6925	0.6731	−0.0194	0.0026
HF	1.4411	1.4507	0.0053	0.2996	0.2953	−0.0043	0.0053
$HCCl_3$[b]	1.3418	1.3607	0.0189	0.7045	0.6806	−0.0239	−0.0050

[a] Difference (dimer−monomer). [b] Complex of chloroform with fluorobenzene.

TABLE 6: Topological Properties of the Electron Density at (3,−1) Critical Point of the C−H Bond in the Isolated Monomer (m) and in the Complex (d)

molecule	form	ρ	$\nabla^2\rho$	λ_1	λ_2	λ_3
CH_4	m	0.2803	−0.9908	−0.7181	−0.7181	0.4455
	d	0.2824	−1.0118	−0.7307	−0.7307	0.4496
$HCCl_3$	m	0.3028	−1.2214	−0.8586	−0.8586	0.4959
	d	0.3062	−1.2762	−0.8832	−0.8832	0.4903
C_6H_6	m	0.2853	−1.0399	−0.7516	−0.7392	0.4509
	d	0.2899	−1.0821	−0.7753	−0.7633	0.4564
HCCH	m	0.2918	−1.1637	−0.7921	−0.7921	0.4205
	d	0.2930	−1.1939	−0.8077	−0.8077	0.4215
HCN	m	0.2914	−1.2067	−0.8148	−0.8148	0.4229
	d	0.2917	−1.2407	−0.8298	−0.8298	0.4189
HF	m	0.3715	−2.6333	−2.3254	−2.3254	2.0175
	d	0.3658	−2.6611	−2.3238	−2.3238	1.9866
$HCCl_3$[a]	m	0.3028	−1.2214	−0.8586	−0.8586	0.4959
	d	0.3164	−1.3984	−0.9271	−0.9269	0.4557

[a] Complex of chloroform with fluorobenzene.

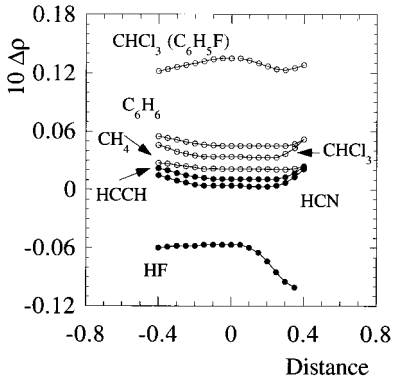

Figure 3. Profiles of electron density difference (au) computed as the difference between the electron density of the monomer in the dimer and that of the isolated monomer along the bond path associated with the C−H bond as the distance (au) from the (3,−1) critical point is enlarged. The origin of distance is located at the bond critical point.

two effects is rather comparable: whereas the distance BCP−carbon is elongated by 0.005−0.022 au, the distance BCP−hydrogen is reduced by 0.004−0.028 au. It is worth noting, however, that the relative magnitude of these two effects is different in those compounds exhibiting anti-H bond behavior with regard to those forming normal H bond complexes. Thus, the shortening of the distance BCP−hydrogen in CH_4, $CHCl_3$, and C_6H_6 is 0.0019−0.0065 larger than the elongation of the carbon nucleus from the BCP, leading to a net reduction in the bond length, as stated in Table 1. Contrarily, the reverse trend is observed in HCCH, HCN, and HF, the net effect being the increase in the bond length (see Table 1).

The values of the electron density at the (3,−1) critical point and its associated properties are given in Table 6. The electron density is sensibly larger than the value obtained for the intermolecular (3,−1) critical point (see Table 2). Indeed, in contrast to the positive values of the laplacian reported in Table 2, the laplacian is negative, which indicates that there is a concentration of charge density between the bonded atoms, as expected for a covalent interaction. In all cases, the laplacian becomes more negative upon formation of the complex, the magnitude of this effect ranging from −0.021 (CH_4) to −0.055 ($CHCl_3$; −0.177 for the complex with fluorobenzene) au. This change in the laplacian arises mainly from an increase (in absolute value) of the curvatures in the directions normal to the bond path (λ_1, λ_2). The only exception is the complex of benzene with HF because the main change is associated with the curvature along the bond path (λ_3), which decreases upon formation of the complex. This effect is also observed in the two other polar compounds considered here, $CHCl_3$ and HCN, whereas the reverse trend is found for CH_4, C_6H_6, and HCCH.

The results in Table 6 show that the electron density at the bond critical point is enlarged upon complexation in all cases, but for HF, where the electron density at the (3,−1) critical point of the H−F bond is 0.0057 au lower in the complex than in the isolated monomer. This effect is also found in the C_s optimized structures of the benzene complexes with methane and hydrogen fluoride: whereas the electron density at the bond critical point of the C−H bond in the complex with methane is enlarged 0.0021 au, that of the F−H bond in the complex with hydrogen fluoride decreases by 0.0064 au. Such a change in the electron density at the bond critical point extends over a wide region around the bond critical point, as can be seen in Figure 3, which shows the profiles of electron density difference ($\rho_{C-H;complex} - \rho_{C-H;isolated\ monomer}$) along the C−H bond as the distance from the bond critical point is increased.

More interestingly, inspection of Figure 3 reveals that the electron density difference profiles for the different compounds are roughly parallel in the interval ±0.4 au from the bond critical point. The largest changes in electron density are found for $CHCl_3$ (complexed to fluorobenzene), where the electron density at the bond critical point is enlarged by >0.01 au, and for HF, where it is reduced by near 0.06 au. Moreover, there is a gradual variation in the electron density for the benzene complexes with the different carbon proton donors, the change in electron density at the (3,−1) critical point being reduced from 0.0046 au for C_6H_6 to only 0.0003 au for HCN (see Table 6).

Because the electron density at the bond critical point provides a measure of the bond order,[7e,13,15] one can reasonably assume that the change in electron density at the bond critical point induced upon complexation gives a measure of the variation in the strength of the bond. Accordingly, such a change can be expected to reflect at least qualitatively the shifts in bond length and stretching frequency for a series of related chemical systems. This can be verified for the benzene complexes with carbon proton donors in Figure 4, which shows significant correlations between the change in electron density at the (3,−1) critical

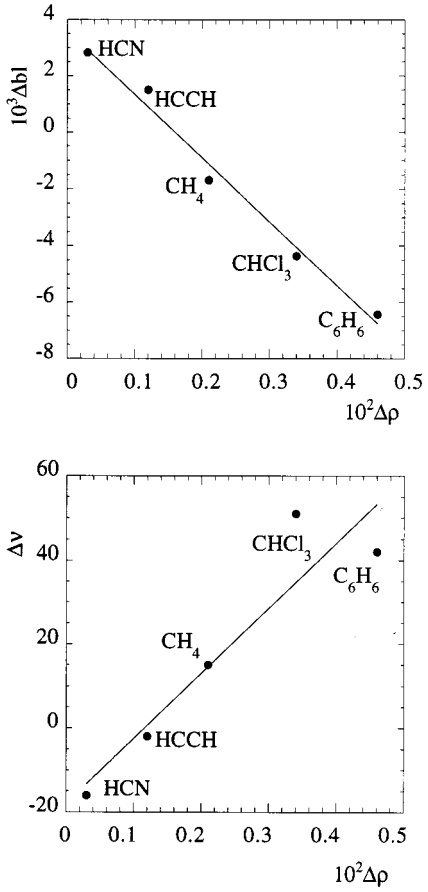

Figure 4. Representation of the shift in bond length (au; top) and stretching frequency (cm^{-1}; bottom) with the change in electron density (au) at the bond critical point of the C−H bond for the benzene complexes with the different carbon proton donors.

point of the C−H bond and the corresponding variations in bond lengths ($r = 0.99$) and stretching frequencies ($r = 0.94$).

The topological analysis already discussed shows no relevant difference for the series of benzene complexes as far as Popelier's criteria for H bonding are concerned. These criteria are focused on the changes in electron density occurring between the hydrogen atom of the donor molecule and the acceptor atom of the interacting partner, as well as on the integrated properties of the hydrogen atom. However, these criteria do not suffice to distinguish between a normal H bond and an anti-H bond complex, which are determined by subtle changes in the electron density of the covalent bond donating the hydrogen atom. These changes are clearly manifested in the increase/decrease of electron density observed in the complexes of fluorobenzene with chloroform and of benzene with hydrogen fluoride, respectively, but even for the related C−H···π benzene complexes a good correlation exists between the change in electron density with the shifts in bond length and vibrational frequency.

Conclusion

The results reported in this study provide a complementary interpretation of the anti-H bonding, which is phenomenologically manifested in the series of benzene complexes examined here as a shortening of the C−H bond length and a blue shift of its stretching frequency. As noted previously by Hobza,[11] such a phenomenon arises from the dominant stabilizing role of the dispersion forces. The results presented here allow us to suggest that the topological criteria proposed by Popelier are not sufficient to characterize such different phenomena as H bonding and anti-H bonding, as demonstrated by the red and blue shift of the respective X−H stretching frequencies. AIM facilitates discrimination between structurally different motifs with and without participation of hydrogen between two heavy atoms. Thus, H bonded criteria based on AIM are satisfied for standard X−H···Y H bonding, nonconventional C−H···O H bonding, and dihydrogen D−H···H−E bonding, and provide a basis to distinguish these interactions from van der Waals interactions of the X···Y type. To differentiate between H bonding and anti-H bonding, our results suggests that it is necessary to supplement those criteria with information on the changes in the electron density of the donor X−H bond occurring upon complexation.

Acknowledgment. We thank Prof. R. W. F. Bader for sending us a copy of PROAIM computer program. This work was supported by the DGICYT under projects PB97-0908 and PB96-1005, and by the Centre de Supercomputació de Catalunya (CESCA; Molecular Recognition Project).

Supporting Information Available: Table listing coordinates and energies are available. This information is available free of charge via the Internet at http://pubs.acs.org.

References and Notes

(1) (a) *Molecular Interactions. From van der Waals to Strongly Bound Complexes*; Scheiner, S., Ed.; Wiley: Chichester, 1997. (b) Adams, H.; Carver, F. J.; Hunter, C. A.; Osborne, N. J. *Chem. Commun.* **1996**, 2529. (c) Adams, H.; Harris, K. D. M.; Hembury, G. A.; Hunter, C. A.; Ivingstone, D.; McCabe, J. F. *Chem. Commun.* **1996**, 2531. (d) Kim, E.; Paliwal, S.; Wilcox, C. S. *J. Am. Chem. Soc.* **1998**, *120*, 11192. (e) Samanta, U.; Chakrabarti, P.; Chandrasekhar, J. *J. Phys. Chem. A* **1998**, *102*, 8964.

(2) Jeffrey, G. A.; Saenger, W. *Hydrogen Bonding in Biological Structures*; Springer: Berlin, 1991.

(3) Karpfen, A.; Yanovitskii, O. *J. Mol. Struct. (THEOCHEM)* **1994**, *314*, 211.

(4) (a) Suhai, S. *J. Chem. Phys.* **1994**, *101*, 9766. (b) Ojamäe, L.; Hermansson, K. *J. Phys. Chem.* **194**, *98*, 4271. (c) Contador, J. C.; Aguilar, M. A.; Sánchez, M. L.; Olivares del Valle, F. J. *J. Mol. Struct. (THEOCHEM)* **1994**, *314*, 229. (d) Estrin, D. A.; Paglieri, L.; Corongiu, G.; Clementi, E. *J. Phys. Chem.* **1996**, *100*, 8701. (e) Chen, W.; Gordon, M. *J. Phys. Chem.* **1996**, *100*, 14136. (f) Cruzan, J. D.; Braly, L. B.; Liu, K.; Brown, M. G.; Loeser, J. G.; Saykally, R. J. *Science* **1996**, *271*, 59. (g) Liu, K.; Brown, M. G.; Cruzan, J. D.; Saykally, R. J. *Science* **1996**, *271*, 62. (i) Gresh, N. *J. Phys. Chem. A* **1997**, *101*, 8680.

(5) (a) Guo, H.; Karplus, M. *J. Phys. Chem.* **1994**, *98*, 7104. (b) Gung, B.; Zhu, Z. *Tetrahedron Lett.* **1996**, *37*, 2189. (c) Zhbankov, R. G. *J. Mol. Struct.* ***1992***, *270*, 523. (d) Jorgensen, W. L.; Damm, W.; Frontera, A.; Lamb, M. L. In *Physical Supramolecular Chemistry*; Echegoyen, L., Kaifer, A. E., Eds.; Kluwer: Amsterdam, 1996; pp 115−126. (e) Luque, F. J.; López, J. M.; López de Paz, M.; Vicent, C.; Orozco, M. *J. Phys. Chem. A* **1998**, *102*, 6690.

(6) (a) Cooney, M.; Czernuszewicz, G.; Postel, E. H.; Flint, S. J.; Hogan, M. E. *Science* **1988**, *241*, 456. (b) Grigoriev, M.; Praseuth, D.; Guieysee, A. L.; Robin, P.; Thuong, N. T.; Harel-Bellan, A. *Proc. Natl. Acad. Sci., U.S.A.* **1993**, *90*, 3501 (c) Sun, J. S.; Garestier, T.; Hélène, C. *Curr. Opin. Struct. Biol.* **1996**, *6*, 327.

(7) (a) Tang, T. H.; Hu, W. J.; Yan, D.; Y.; Cui, Y. P. *J. Mol. Struct. (THEOCHEM)* **1990**, *207*, 319. (b) Atwood, J. L.; Hamada, F.; Robinson, K. D.; Orr, G. W.; Vincent, R. L. *Nature* **1991**, *349*, 683. (c) Suzuki, S.; Green, P. G.; Bumgarner, R. E.; Dasgupta, S.; Goddard, W. A., III.; Blake, G. A. *Science* **1992**, *257*, 942. (d) Pribble, R. N.; Garret, A. W.; Haber, K.; Zwier, T. S. J. Chem. Phys. **1995**, *103*, 531. (e) Cubero, E.; Orozco, M.; Luque, F. J. *J. Phys. Chem. A* **1999**, *103*, 315.

(8) (a) Desiraju, G. R. *Acc. Chem. Res.* **1991**, *24*, 290. (b) Desiraju, G.; Kashino, S.; Coombs, M. M.; Glisker, J. *Acta Crystallogr.* **1993**, *B49*, 880. (c) Kock, U.; Popelier, P. L. A. *J. Phys. Chem.* **1995**, *99*, 9747. (d) Alkorta, I.; Campillo, N.; Rozas, I.; Elguero, J. *J. Org. Chem.* **1998**, *63*, 7759.

(9) (a) Richardson, T. B.; de Gala, S.; Crabtree, R. H.; Siegbahn, P. E. M. *J. Am. Chem. Soc.* **1995**, *117*, 12875. (b) Popelier, P. L. A. *J. Phys. Chem. A* **1998**, *102*, 1873.

(10) (a) Park, S.; Ramachandran, R.; Lough, A. J.; Morris, R. H. *J. Chem. Soc., Chem. Commun.* **1994**, 2201. (b) Peris, E.; Lee, J. C.; Rambo, J. R.; Eisenstein, O.; Crabtree, R. H. *J. Am. Chem. Soc.* **1995**, *117*, 3485. (c) Wessel, J.; Lee, J. C.; Peris, E.; Yap, G. P. A.; Fortin, J. B.; Ricci, J. S.;

Sini, G.; Albinati, A.; Koetzle, T. F.; Eisenstein, O.; Rheingold, A. L.; Crabtree, R. H. *Angew. Chem., Int. Ed. Engl*. **1995**, *34*, 2507. (d) Crabtree, R. H.; Siegbahn, P. E. M.; Eisenstein, O.; Rheingold, A.; Koetzle, T. F. *Acc. Chem. Res.* **1996**, *29*, 348.

(11) Hobza, P.; Spirko, V.; Selzle, H. L.; Schlag, E. W. *J. Phys. Chem. A* **1998**, *102*, 2501.

(12) Hobza, P.; Spirko, V.; Havlas, Z.; Buchhold, K.; Reimann, B.; Barth, H. D.; Brutschy, B. *Chem. Phys. Lett.* **1999**, *299*, 180.

(13) (a) Bader, R. F. W. *Atoms in Molecules. A Quantum Theory;* Oxford University Press: Oxford. 1990. (b) Bader, R. F. W. *Chem. Rev.* **1991**, *91*, 893. (c) Bader, R. F. W. *J. Phys. Chem. A* **1998**, *102*, 7314.

(14) (a) Carroll, M. T.; Chang, C.; Bader, R. F. W. *Mol. Phys*. **1988**, *65*, 695. (b) Destro, R.; Bianchi, R.; Gatti, C.; Merati, F. *Chem. Phys. Lett.* **1991**, *186*, 47. (b) Gonzalez, L.; Mo, O.; Yañez, M.; Elguero, J. *J. Mol. Struct. (THEOCHEM)* **1996**, *371*, 1. (c) Rozas, I.; Alkorta, I.; Elguero, J. *J. Phys. Chem. A* **1997**, *101*, 9457. (d) Alkorta, I.; Rozas, I.; Elguero, J. *Theor. Chem. Acc.* **1998**, *99*, 116. (e) Novoa, J. J.; Lafuente, P.; Mota, F. *Chem. Phys. Lett.*. **1998**, *290*, 519. (f) Luisi, B.; Orozco, M.; Sponer, J.; Luque, F. J.; Cole, J. C.; Shakked, J. Z. *J. Mol. Biol.* **1998**, *279*, 1125.

(15) (a) Boyd, R. J.; Choi, S. C. *Chem. Phys. Lett.*. **1985**, *120*, 80. (b) *ibidem.* **1986**, *129*, 62. (c) Bader, R. F. W.; Tang, T. H.; Tal, Y.; Biegler-König, F. *J. Am. Chem. Soc.* **1982**, *104*, 946. (d) Alkorta, I.; Elguero, J. *J. Phys. Chem.* **1996**, *100*, 19367. (e) Mallinson, P. R.; Wozniak, K.; Smith, G. T.; McCormack, K. L. *J. Am. Chem. Soc.* **1997**, *119*, 11502. (f) Roversi, P.; Barzaghi, M.; Merati, F.; Destro, R. *Can. J. Chem.* **1996**, *74*, 4, 1145. (g) Mo, O.; Yáñez, M.; Elguero, J. *J. Chem. Phys.* **1992**, *97*, 6628. (h) Alkorta, I.; Campillo, N.; Rozas, I.; Elguero, J. *J. Org. Chem.* **1998**, *63*, 7759. (i) Alkorta, I.; Rozas, I.; Elguero, J. *Struct. Chem.* **1998**, *9*, 243.

(16) Møller, C.; Plesset, M. S. *Phys. Rev.* **1934**, *46*, 618.

(17) Hariharan, P. C.; Pople, J. A. *Theor. Chim. Acta* **1973**, *28*, 213.

(18) Boys, S. F.; Bernardi, F. *Mol. Phys.* **1970**, *19*, 553.

(19) Gaussian 94 (Rev. A.1). Frisch, M. J.; Trucks, G. W.; Schlegel, H. B.; Gill, P. M. W.; Johnson, B. G.; Robb, M. A.; Cheeseman, J. R.; Keith, T. A.; Petersson, G. A.; Montgomery, G. A.; Raghavachari, K.; Al-Laham, M. A.; Zakrzewskim V. G.; Ortiz, J. V.; Foresman, J. B.; Cioslowski, J.; Stefanov, B. B.; Nanayakkara, A.; Challacombe, M.; Peng, C. Y.; Ayala, P. Y.; Chen, W.; Wong, M. W.; Andres, J. L.; Replogle, E. S.; Gomperts, R.; Martin, R. L.; Fox, D. J.; Binkley, J. S.; Defrees, D. J.; Baker, J.; Stewart, J. J. P.; Head-Gordon, M.; Gonzalez, C.; Pople, J. A. Gaussian. Inc.; Pittsburgh, PA, 1995.

(20) Biegler-König, F.; Bader, R. F. W.; Tang, T. H. *J. Comput. Chem.* **1982**, *3*, 317.

(21) Let us note that the cage critical point is surrounded by two ring critical points: one corresponds to the ring critical point formed near C1, the carbon atom bearing the fluorine atom, and the other is the ring critical point of the benzene ring.

(22) The values of the density and the laplacian at the bond critical points of the C_s minimum energy structures are (in atomic units) $\rho = 0.0052, \nabla^2\rho = 0.0171$ and $\rho = 0.0110, \nabla^2\rho = 0.0349$ for the benzene complexes with methane and hydrogen fluoride, respectively.

4.2.2 C-H···O contacts in the adenine·uracil Watson-Crick and uracil·uracil nucleic acid base pairs: Nonempirical ab initio study with inclusion of electron correlation effects

Pavel Hobza, Jiří Šponer, **Elena Cubero**, Modesto Orozco & F. Javier Luque

J. Phys. Chem. B. **2000**, *104*, 6286-6292

(Esta página está intencionadamente en blanco)

C−H···O Contacts in the Adenine···Uracil Watson−Crick and Uracil···Uracil Nucleic Acid Base Pairs: Nonempirical ab Initio Study with Inclusion of Electron Correlation Effects

Pavel Hobza,*,† Jiří Šponer,† Elena Cubero,‡ Modesto Orozco,‡ and F. Javier Luque§

J. Heyrovský Institute of Physical Chemistry, Academy of Sciences of the Czech Republic, 182 23 Prague 8, Czech Republic, Departament de Bioquímica i Biologia Molecular, Facultat de Química, Universitat de Barcelona, Martí i Franqués 1, 08028 Barcelona, Spain, and Departament de Fisicoquímica, Facultat de Farmàcia, Universitat de Barcelona, Av. Diagonal s/n, 08028 Barcelona, Spain

Received: February 23, 2000

Structures and stabilities of H-bonded adenine···uracil Watson−Crick (AU WC) and two uracil···uracil nucleic acid base pairs possessing C−H···O contacts (UU7, UU−C) were determined using gradient optimization with inclusion of electron correlation via the second-order Møller−Plesset (MP2) perturbational method with a 6-31G** basis set of atomic orbitals. In the AU WC pair, closest contacts occur between the N6(A) and O4(U), N1(A) and N3(U), and C2(A) and O2(U) atoms: 2.969, 2.836, and 3.568 Å, respectively. For the UU7 pair the closest contact corresponds to O4···N1 and C5···O2 pairs with distances of 2.860 and 3.257 Å, respectively, while in UU−C pair the closest contact was found for O4···N3 and C5···O4 heteroatoms with distances of 2.913 and 3.236 Å, respectively. The nature of all intermolecular contacts in the sense of a conventional H-bonding or improper, blue-shifting H-bonding was determined on the basis of harmonic vibrational analysis, atom-in-molecules (AIM) Bader analysis of electron density, and natural bond orbital analysis (NBO) performed at the MP2/6-31G** level of theory. N−H stretch frequencies of A and U exhibited a red shift and intensity decrease upon formation of AU WC base pair. It unambiguously proves the existence of the N−H···O and O···H−N H-bonds. The frequency shift of the C−H stretching frequency of A upon complex formation is, however, marginal ($\sim$2 cm^{-1}). Bader AIM analysis and NBO analysis confirmed the existence of N−H···O and O···H−N H-bonds in the AU WC pair but was inconclusive in the case of C−H···O contact. The results thus clearly show that the C2−H2···O2 contact in the AU or AT WC base pair corresponds neither to standard H-bond nor to improper, blue-shifting H-bond. The opposite result, however, has been found for the UU pairs; here the vibrational analysis shows a red shift and intensity increase of both N−H and C−H stretching vibrational frequencies upon the formation of the pair. This is a clear manifestation of the presence of two H-bonds of the N−H···O and O···H−C types. Bader AIM analysis as well as NBO analysis confirmed the existence of both H-bonds.

1. Introduction

Hydrogen bonds (H-bonds) determine the three-dimensional structures of biomacromolecules and are therefore one of the key interactions in molecular biology. Most of the H-bonds are of X−H···Y types, where X is an electronegative atom and Y is either an electronegative atom with lone electron pair(s) or a region of excess of electron density. H-bonds where X and Y are F, O, or N atoms are well-known,[1,2] and the same is now true also for H-bonds with Y being aromatic π-electrons.[3−5] Already in 1982, a survey of crystal structures established the existence of C−H···O H-bonds[6] and extensive literature was devoted to this subject.[1,2,7] The C−H···O H-bonds are believed to be weak, and the question arises whether all C−H···O contacts correspond to standard H-bonds. Recently we suggested a new type of intermolecular bonding, termed improper, blue-shifting H-bonding,[8,9] with spectral manifestations quite opposite to those of H-bonding. (We called originally this bonding anti-H-bonding. This term was rightfully criticized as misleading mainly because it might contradict the existence of binding between both subsystems or it could evoke a complex with antihydrogen.) Instead of elongation of the X−H bond accompanied by a red shift of the X−H stretching frequency (typical for H-bonding), the improper, blue-shifting H-bonding is characteristic by contraction of the X−H bond and a blue shift of the respective X−H stretching frequency. The C−H···π improper, blue-shifting H-bonding was theoretically predicted and later detected by double-resonance ion-depletion infrared spectroscopy.[9] Theoretical prediction was based on geometrical characteristics obtained from standard and counterpoise (CP)-corrected geometry optimizations and vibrational frequencies determined by harmonic and anharmonic vibrational analysis. Analysis of the electron density topology obtained from atom-in-molecules (AIM) Bader theory[10] suggests that the specific features of the improper H-bonds originates from redistribution of electron density in the C−H bond induced upon complexation.[11] Specifically, the electron density at the bond critical point (bcp) increased if an improper H-bond is formed while it decreased if a standard H-bond is formed.[11] The family of improper, blue-shifting H-bonds was recently extended to improper H-bonds of the C−H···O type, and the C−H···O improper H-bond in fluoroform···ethylene oxide[12] was manifested by 0.1

* Corresponding author. Fax: 420 2 858 2307. E-mail: hobza@indy.jh-inst.cas.cz.
† Academy of Sciences of the Czech Republic.
‡ Facultat de Quimica, Universitat de Barcelona.
§ Facultat de Farmàcia, Universitat de Barcelona.

10.1021/jp0007134 CCC: $19.00 © 2000 American Chemical Society
Published on Web 06/10/2000

pm contraction of C−H bond and significant (∼30 cm^{-1}) blue shift of the C−H stretching frequency accompanied by lowering of intensity of the respective vibration. Also in this case the Bader AIM theory predicted[13] an increase in the C−H electron density induced upon complexation which justifies the shortening of the C−H bond and the respective blue shift in the C−H stretch frequency.

A very large blue shift of the C−H stretch frequency, more than 100 cm^{-1}, was detected recently from infrared spectra of $X^-\cdots H_3CY$ ionic complexes (X = Cl, Y = Br; X, Y = I), which were also thoroughly investigated theoretically.[14] Contrary to the halogen substituents, for Y = H, methane displays a red shift upon complexation with both anions. The natural bond orbital (NBO) analysis was used[14] for explaining the different origin of bonding in these ion−molecule complexes. It was demonstrated that formation of H-bonds in $X^-\cdots$methane complexes is accompanied by electron density transfer (EDT) from halide anion lone pairs to the C−H σ^* antibonding orbitals. Formation of improper H-bonds in the $X^-\cdots H_3CY$ complexes is accompanied, on the other hand, with an EDT to C−Y σ^* antibonding orbital. Let us finally mention that the EDT concept of H-bonding using NBO analysis was introduced by Reed, Curtiss, and Weinhold.[15]

X−H···Y H-bonds with X and Y being N and O are well-known in nucleic acid base pairing and contribute significantly to the stability of a pair. The C−H···O contacts in nucleic acid base pairs are less frequent and mostly exist as base−backbone contacts between purine C8−H or pyrimidine C6−H and the O5′ atom in the backbone[16] when the bases are in the anti-conformation. There are, however, also C−H···O base−base contacts. Such contacts occur also in AT/U WC or Hoogsteen pairs. Conventionally, the AT/U WC pair which exist in the crystal of DNA/RNA is linked by two H-bonds of the N−H···O and N···H−N type which correspond to close N···O and N···N contacts. Hunter and co-workers[17] speculated recently that the third long C···O contact in the AU WC pair might correspond to a third H-bond which would contribute to the stability of the pair. This idea was supported by Starikov and Steiner;[18] they considered this interaction "*cum grano salis* as a weak H-bond." Another example of the C−H···O contact was found recently in the uracil···uracil base pair, referred to as the Calcutta pair. The Calcutta pair discovered in the crystal structure of RNA[16] was believed to have a conventional N3−H···O4 and an unconventional C5−H···O4 H-bond.

Recently, the potential energy surface of isolated uracil dimer in the gas phase was investigated[19] in our laboratory using molecular dynamics/quenching techniques and ab initio calculations. The simulations revealed that the Calcutta pair (designated UU−C) is not significantly populated in the gas phase, since its stabilization energy is rather low. However, another structure (designated as UU7) with the C−H···O contact was found to be quite populated. Besides the C−H···O contact, the structure was stabilized by an N1−H···O H-bond; this H-bond is considerably stronger than N−H···O bonds involving N3 atom. However, the UU7 pair cannot occur in nucleic acids since the N1 position is not accessible to H-bonding. Because both UU7 and UU−C pairs are important, we included both of them in the present analysis.

The aim of the study is clarify the nature of C−H···O contacts occurring in the AU WC, UU−C, and UU7 base pairs and specify whether they correspond to H-bonds, improper H-bonds, or other types of interactions. Among other calculations we report the first MP2 vibrational analysis of DNA base pairs, supplemented by Bader analysis of the electron densities and NBO analysis. Both analyses were performed at the correlated MP2 level. The calculations clearly identify the existence of the C−H···O H-bond in the UU base pairs while we have found no justification to speculate about a third H-bond in AU and AT WC base pairs.

2. Calculations

The geometries of AU WC and UU pairs and monomers were optimized at the Hartree−Fock (HF) level using the 6-31G** basis set[20] and at correlated second-order Møller−Plesset level (MP2) with the same basis set. The frozen core approximation was adopted in MP2 calculations. No symmetry constraint was considered in the optimization. The final stabilization energy for the optimized complex was determined by correcting for the basis set extension effects, which were eliminated using the Boys−Bernardi counterpoise method.[21] Further, the deformation energies of bases upon complexation were subtracted; these were calculated as the difference of the energies of the optimized bases and the energies of bases with the same geometry as within the complex. It means that structure of a complex was optimized at a standard potential energy surface (PES), i.e., without counterpoise corrections and not at the theoretically more justified CP-corrected PES. The structure of the AT WC pair was therefore re-optimized by the CP-corrected gradient optimization[22] at the HF/6-31G** level, to show that the explicit inclusion of BSSE in the course of the optimization does not change the results qualitatively. In CP-corrected optimizations the basis set superposition error is eliminated in each gradient cycle. Harmonic vibrational frequencies were determined using Wilson's FG analysis. We have shown previously[23] that harmonic intermolecular vibrational frequencies of the AT WC pair agree well with the corresponding anharmonic frequencies. All the calculations were performed with the GAUSSIAN 94[24] and GAUSSIAN 98[25] codes.

The electron density topological analysis was carried out using the theory of atoms in molecules,[10] which has been successfully used to characterize H-bonds in a variety of molecular complexes.[26] Calculations were performed using the molecular structures optimized at the MP2 level. Attention was focused on the properties of the (3,−1) bond critical points and on selected integrated atomic properties of the hydrogen atoms participating in H-bond interactions. Calculations were conducted with the program PROAIM.[27]

3. Results and Discussion

3.1. Geometries, Energies, and Vibrational Analysis. Structures and atom numbering of optimized AU WC, UU7, and UU−C base pairs are shown in Figure 1, and the respective geometrical, vibrational, and energetical characteristics are presented in Table 1.

The MP2 stabilization energies for both pairs are larger than the HF values, because the MP2 method includes the dispersion energy neglected within the HF approximation. Note that the UU7 base pair is considerably more stable than the UU−C one and is at least partly competitive with those UU pairs which are stabilized by two N−H···O H-bonds.[19] Thus the pair is expected to be detectable in gas-phase experiments, in contrast to UU−C.[19]

The intersystem distances obtained at the MP2 optimization are shorter than the HF ones, consistent with MP2 optimizations reported earlier for selected pyrimidine base pairs.[28] The reason is obviously the neglect of dispersion attraction by the HF method. Let us first discuss the more accurate MP2 characteristics. Analyzing the non-hydrogen atom distances in the AU

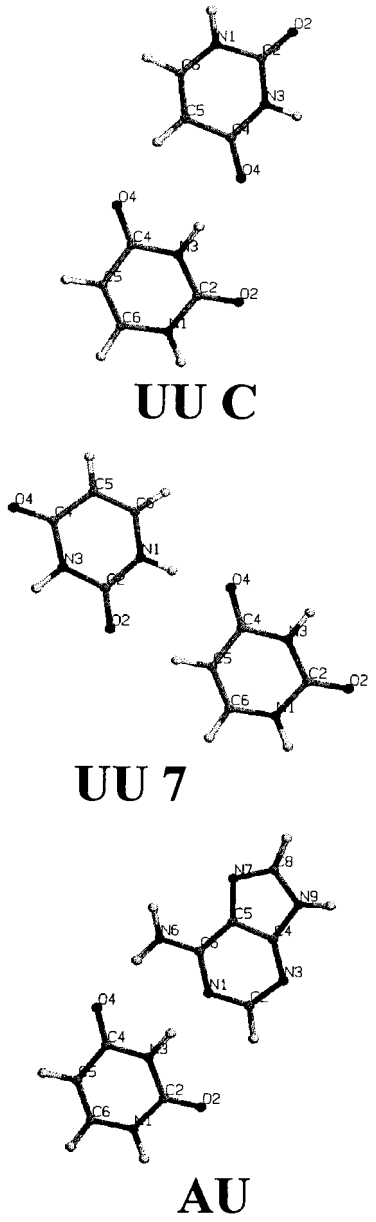

Figure 1. Structures and atom numbering of AU WC, UU7, and UU−C base pairs.

WC pair, we found that the C2−O2 distance (3.57 Å) is considerably longer than the N6−O4 and N1−N3 distances (2.97 and 2.84 Å). Further, the C2−H2 covalent bond length is practically unchanged upon complex formation while the N6−H6 bond and especially N3−H3 bond are significantly elongated. The calculated shifts in X−H stretching vibration frequencies upon the formation of the complex agree with the geometrical results. The largest red shift was found for the N3−H3 stretching frequency of uracil (618 cm^{-1}). Also the N6−H6 amino stretching vibration frequency of adenine shows a large, though considerably smaller red shift upon the formation of the base pair (145 cm^{-1}) while the C2−H2 stretching frequency of adenine is practically unchanged by the complex formation. All these data are consistent with the existence of strong N3−H3···N1 and moderate N6−H6···O4 H-bonds. There is, however, no evidence of formation of either an H-bond or improper H-bond in the case of C2−H2···O2 contacts. The HF results agree basically with the MP2 values giving evidence about the dominant role of electrostatic interaction. The relative changes of distances and vibrational frequencies are at the HF level consistently smaller since the base pair strength is undervaluated.

The role of CP-corrected optimization was studied for the AT WC pair. We performed standard and CP-corrected HF/6-31G** gradient optimization for this pair and found that in both cases optimization led to a planar structure. The CP-corrected optimization resulted in slightly larger intermolecular separations: N1−N3 and N6−O4 distances increased by 0.055 and 0.005 Å, respectively. The changes of N6−H6, N3−H3, and C2−H2 bonds upon complex formation remain, however, the same as in standard gradient optimization. It indicates that the basis set extension artifact does not influence the results substantially.

The situation with the UU7 base pair is different. The C5−O2 distance (3.26 Å) is again longer than that of O4−N1 (2.86 Å), but the C···O contact is considerably shorter than that in the AU WC pair. Also other geometrical and vibrational data are consistent with the existence of two H-bonds of the N1−H1···O4 and C5−H5···O2 type. The former H-bond is stronger than the N6−H6···O4 H-bond in the AU WC pair and is characterized by a red shift of 288 cm^{-1}. The red shifts of symmetrical and antisymmetrical C5−H5 stretching frequencies are considerably smaller (34 and 5 cm^{-1}) but clearly supporting the existence of a C−H···O H-bond. It should be mentioned that at the HF level we obtained for these frequencies red and blue shifts of 32 and 23 cm^{-1}, respectively. It shows that for a quantitative analysis of base pairing the electron correlation should be included. The C5−O4 and O4−N3 distances (3.24 and 2.91 Å) in UU−C are similar to those in the UU7, and these contacts are consistent with the existence of two H-bonds of the C5−H···O4 and N3−H···O4 type. They are characterized by elongation of N3−H and C5−H bonds by 0.014 and 0.002 Å what is similar to those found in N−H···N and C−H···O bonds in UU7. For the UU−C we did not performed the MP2 harmonic vibrational analysis.

3.2. Electron Density Topological Analysis. *AU WC Base Pair*. The formation of the AU WC complex gives rise to the appearance of five critical points (see Figure 2). Three are (3,−1) critical points linking the atoms H6(A) and O4(U), N1-(A) and H3(U), and H2(A) and O2(U). The other two are (3,+1) critical points appearing between the bond critical points. Table 2 gives the topological properties of the (3,−1) critical points formed upon dimerization. The electron density at the bond critical points varies from 0.0059 to 0.0434 au. These values are within the range determined for similar H-bonded complexes, which typically varies from 0.002 to 0.04 au.[26a,29] The value for the H2···O2 interaction (0.0059 au) is sensibly lower than that for the H6···O4 (0.0251 au) and N1···H3 (0.0434 au) interactions, in agreement with the differences in geometrical distances for the intermolecular contacts (see above and Table 1). As expected for closed-shell interactions, the Laplacian of the electron density is positive, which indicates a depletion of electron density from the interatomic surface toward the interacting nuclei, as noted in the positive value of λ_3, which is much larger than the other two eigenvalues.

An additional indication of the strength of the intermolecular contacts comes from comparison of the penetration effects between the H-bond acceptor and hydrogen atoms, which can be measured from the difference between atomic radii for the bonded and nonbonded monomers. In the bonded complex the atomic radius is determined as the distance to the intermolecular bond critical point from the atom, and in the isolated monomer it is estimated as the distance from the atom to an isodensity

TABLE 1: Stabilization Energies[a] (ΔE), Intermolecular X−Y Distances[b] (r), and Changes of X−H Distances[b] (Δr) and Vibration Stretching Frequencies[c] ($\Delta\nu$) upon Formation of a Complex in the AU WC, UU7, and UU−C Pairs Determined at the HF/6-31G and MP2/6-31G** Levels**

complex[d]	level	ΔE	$r(N_6-O_4)$	$\Delta r/\Delta\nu(N_6-H_6)$	$r(N_1-N_3)$	$\Delta r/\Delta\nu(N_3-H_3)$	$r(C_2-O_2)$	$\Delta r/\Delta\nu(C_2-H_2)$
AU WC	HF	9.8	3.083	0.007/−43[e], −84[f]	2.989	0.016/−320	3.780	0/+9
	MP2	12.1	2.969	0.009/−32[e], −145[f]	2.836	0.045/−618	3.568	0/−2

complex[d]	level	ΔE	$r(O_4-N_1)$	$\Delta r/\Delta\nu(N_1-H_1)$	$r(C_5-O_2)$	$\Delta r/\Delta\nu(C_5-H_5)$
UU7	HF	9.9	2.946	0.010/−179	3.398	0.002/ +23[e], −32[f]
	MP2	11.5	2.860	0.016/−288	3.257	0.003/−5[e], −34[f]

complex[d]	level	ΔE	$r(O_4-N_3)$	$\Delta r(N_3-H_3)$	$r(C_5-O_4)$	$\Delta r(C_5-H_5)$
UU−C	MP2	8.1	2.913	0.014	3.236	0.002

[a] Energies in kcal/mol. [b] Distances in Å. [c] Vibration frequencies in cm^{-1}. [d] Cf. Figure 1. [e] Antisymmetrical vibration. [f] Symmetrical vibration.

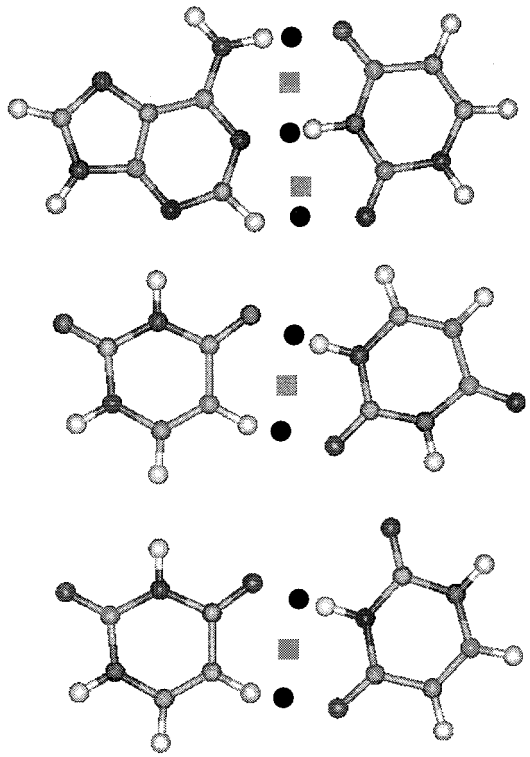

Figure 2. Representation of the bond (circle) and ring (square) critical points formed in the adenine−uracil (top) complex and in the two uracil (UU7, middle; UU−C, bottom) dimers.

contour (a value of 0.001 au has been adopted here) in the direction of the hydrogen bond. The results in Table 2 indicate a mutual penetration of the interacting H-bond acceptor and hydrogen atoms varying between 1.0 and 1.3 Å for the N6−H6···O4 and N3−H3···N1 contacts. Nevertheless, this effect is clearly less important for the C2−H2···O2 contact, which agrees with the largest interatomic distance (see Table 1).

Table 2 also gives the topological properties for the (3,−1) critical points of the N−H and C−H bonds involved in hydrogen-bond interactions in the dimer, as well as in the isolated monomers. The values of the electron density at these critical points are larger by roughly 1 order of magnitude than the electron densities of the intermolecular (3,−1) critical points, as expected from the covalent nature of the bonds. The dimerization decreases the electron density at the intramolecular (3,−1) critical point of N6−H6 and N3−H3 bonds by around 0.012 and 0.032 au, as occurs for conventional hydrogen bonds. Nevertheless, the electron density in the C2−H2 bond remains nearly unaffected.

According to Popelier's criteria for hydrogen bonding,[26] the hydrogen atoms involved in hydrogen bonding exhibit similar changes in selected integrated atomic properties, which are (i) an increase in the net charge, (ii) a lowering in the in the absolute value of the atomic energy, (iii) a reduction in the first moment, and finally (iv) a decrease in the atomic volume. All these trends are found for the hydrogen atoms in the X−H bonds that participate in intermolecular interactions, as can be seen from inspection of Table 3. For the N−H bonds, the net charge is increased by around 0.009 units of electron, the atomic energy decreases in absolute value by 0.05 au, the first moment is reduced by around 0.04 au, and the atomic volume is diminished by around 11 au. These changes are significantly less marked for the hydrogen atom of the C2−H2 bond.

UU Pairs. The formation of the two uracil dimers gives rise to the appearance of three critical points (see Figure 2). Two are (3,−1) bond critical points between atoms O4···H1 and H5···O2 in UU7 and O4···H3 and H5···O4 in UU−C, and the other is a ring critical point located between the two intermolecular (3,−1) critical points. The topological properties of the electron density at the (3,−1) critical points in O4···H1 (UU7) and O4···H3 (UU−C), as well as in H5···O2 (UU7) and H5···O4 (UU−C), are very similar (Table 4), despite the different stabilization energy of the corresponding complexes (see Table 1).

The electron density at the (3,−1) critical points (Table 4) lies within the expected range for similar interactions.[26a,29] They are, however, larger than the values found for the H6···O4 and H2···O2 bonds in the AU WC pair (see Table 1). Indeed, the mutual penetration of the hydrogen-bond acceptor and hydrogen atoms (Table 3) is slightly larger for the UU pairs than for the corresponding contacts in the AU dimer. This effect is particularly relevant in the H5···O2 (UU7) and H5···O4 (UU−C) bonds compared to the H2···O2 contact (AU), since the mutual penetration in the two former cases is around 0.4 Å larger than for the corresponding contact in AU. The electron density at the N1−H1 (UU7) and N3−H3 (UU−C) bonds is reduced upon dimerization by ∼0.016 au, and the electron density at the C5−H5 bond is increased by ∼0.002 au. These changes are larger than the corresponding variations observed for the N6−H6 and C2−H2 bonds in the AU pair.

Table 5 shows the changes in the integrated atomic properties for the hydrogen atoms involved in hydrogen bonding for the UU pairs. Again, all the changes follow the expected trends pointed out by Popelier.[26] Importantly, the changes experienced by the hydrogen atom in the C5−H5 bond are sensibly larger than those found for the hydrogen atom in the C2−H2 bond in the AU dimer (see Table 3).

Bond Order−Bond Length Relationships. The dependence between the intermolecular distance and the logarithm of the

TABLE 2: Electron Density Topological Properties[a] at the (3,−1) Critical Points for the X−H···Y Contacts Formed upon Complexation between Adenine and Uracil and at the (3,−1) Critical Points of the Participating X−H Bonds in the Dimer and in the Isolated Monomers

bond	ρ	$\nabla^2\rho$	λ_1	λ_2	λ_3	Δr_H	Δr_Y	$\Delta r_H + \Delta r_Y$
			AU WC Intermolecular Bonds					
H6···O4	0.0251	0.0710	−0.0321	−0.0315	0.1346	0.503	0.503	1.006
N1···H3	0.0434	0.1003	−0.0673	−0.0641	0.2317	0.609	0.714	1.323
H2···O2	0.0059	0.0214	−0.0055	−0.0052	0.0321	0.265	0.132	0.397
			AU WC Intramolecular Bonds					
N6−H6	0.3305	−1.7893	−1.3580	−1.2993	0.8679			
N3−H3	0.3075	−1.6375	−1.2771	−1.2371	0.8768			
C2−H2	0.2956	−1.1564	−0.8339	−0.7961	0.4737			
			A Bonds					
N6−H6	0.3426	−1.8228	−1.3270	−1.2612	0.7655			
C2−H2	0.2942	−1.1309	−0.8216	−0.7823	0.4730			
			U Bonds					
N3−H3	0.3394	−1.8288	−1.3395	−1.2842	0.7949			

[a] Properties are electron density (ρ) and its Laplacian ($\nabla^2\rho$) and eigenvalues (λ); penetration effects are determined from the difference between nonbonded and bonded radii (Δr).

TABLE 3: Integrated Atomic Properties[a] for the Hydrogen Atoms in the X−H Bonds Involved in Hydrogen Bonding in the Adenine−Uracil Pair and in the Respective Isolated Monomers with the Change for a Given Property in the Dimer Relative to the Isolated Monomer Given in Parentheses

atoms	q	E	$\|M\|$	V
		AU WC Bonds		
(N6)H6	0.530 (+0.090)	−0.3894 (+0.0504)	0.133 (−0.043)	17.67 (−10.13)
(N3)H3	0.555 (+0.086)	−0.3670 (+0.0560)	0.118 (−0.048)	14.54 (−12.11)
(C2)H2	0.058 (+0.037)	−0.6185 (+0.0158)	0.113 (−0.013)	44.52 (−3.15)
		A Bonds		
(N6)H6	0.441	−0.4398	0.176	27.80
(C2)H2	0.021	−0.6343	0.126	47.67
		U Bonds		
(N3)H3	0.469	−0.4230	0.166	26.65

[a] All values in atomic units: q, net charge; E, energy; M, first moment; V, volume.

TABLE 4: Electron Density Topological Properties[a] at the (3,−1) Critical Points for the X−H···Y Contacts Formed upon Formation of the Two Uracil Dimers and at the (3,−1) Critical Points of the Participating X−H Bonds in the Dimer and in the Isolated Monomers

bond	ρ	$\nabla^2\rho$	λ_1	λ_2	λ_3	Δr_H	Δr_Y	$\Delta r_H + \Delta r_Y$
			UU7 Intermolecular Bonds					
O4···H1	0.0323	0.0956	−0.0455	−0.0442	0.1853	0.556	0.556	1.112
H5···O2	0.0164	0.0467	−0.0182	−0.0182	0.0831	0.477	0.397	0.874
			W7 Intramolecular Bonds					
N1−H1	0.3269	−1.7757	−1.3580	−1.3085	0.8908			
C5−H5	0.2892	−1.1228	−0.7973	−0.7755	0.4500			
			UU−C Intermolecular Bonds					
O4···H3	0.0285	0.0841	−0.0385	−0.0377	0.1602	0.535	0.533	1.068
H5···O4	0.0166	0.0477	−0.0186	−0.0184	0.0847	0.475	0.401	0.876
			W−C Intramolecular Bonds					
N3−H3	0.3244	−1.7632	−1.3391	−1.2934	0.8693			
C5−H5	0.2896	−1.1247	−0.7984	−0.7767	0.4504			
			U Bonds					
N1−H1	0.3431	−1.8486	−1.3560	−1.2948	0.8022			
N3−H3	0.3394	−1.8288	−1.3395	−1.2842	0.7949			
C5−H5	0.2874	−1.0690	−0.7720	−0.7476	0.4506			

[a] See footnote in Table 2.

electron density at the bond critical point, which can be used as a measure of the bond order,[30] is given in Figure 3 for the seven intermolecular bond critical bonds in the AU and UU pairs. Inspection of Figure 3 shows the existence of a linear relationship between the interatomic H···X distance (d) and the logarithm of the electron density (ρ) ($d = 0.16-0.50 \ln \rho$; $r = 0.99$), which agrees with previous bond order−bond length relationship studies in similar H-bonded complexes.[11,26g,29,30,31]

Comparison of the changes in bond lengths and vibrational stretching frequencies for the X−H bonds upon complexation in the AU and UU pairs is made in Figure 4. There is a relationship between the change in the electron density at the (3,−1) critical point of the X−H bond and the variation in either the bond length or the vibrational frequency. Nevertheless, there is a subtle difference in the behavior observed for N−H and C−H bonds. In the former case, there is a depletion in the electron density at the N−H bond critical point upon complexation (see Tables 2 and 4), which is larger as the interatomic distance becomes smaller: this effect decreases in the order N3−H3 (AU) > N1−H1 (UU7) > N3−H3 (UU−C) >

TABLE 5: Integrated Atomic Properties[a] for the Hydrogen Atoms in the X−H Bonds Involved in Hydrogen Bonding in the Two Uracil Dimers and in the Respective Isolated Monomers with the Change for a Given Property in the Dimer Relative to the Isolated Monomer Given Parentheses

atoms	*q*	*E*	|*M*|	*V*
		UU7 Bonds		
(N1)H1	0.544 (+0.078)	−0.3833 (+0.0442)	0.123 (−0.043)	16.05 (−10.45)
(C5)H5	0.130 (+0.083)	−0.5797 (+0.0331)	0.091 (−0.031)	36.86 (−9.49)
		UU−C Bonds		
(N3)H3	0.543 (+0.074)	−0.3813 (+0.0417)	0.125 (−0.041)	16.64 (−10.01)
(C5)H5	0.128 (+0.081)	−0.5813 (+0.0315)	0.092 (−0.030)	36.97 (−9.38)
		Uracil Bonds		
(N1)H1	0.467	−0.4275	0.166	26.50
(N3)H3	0.469	−0.4230	0.166	26.65
(C5)H5	0.047	−0.6128	0.122	46.35

[a] See footnote in Table 3.

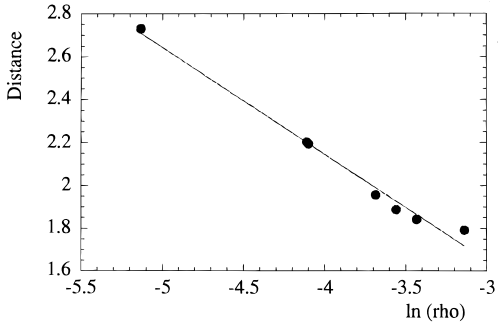

Figure 3. Representation of the change in the interatomic H···X distance (Å) vs the variation in the logarithm of the electron density at the corresponding bond critical point for the adenine−uracil complex and the two uracil dimers.

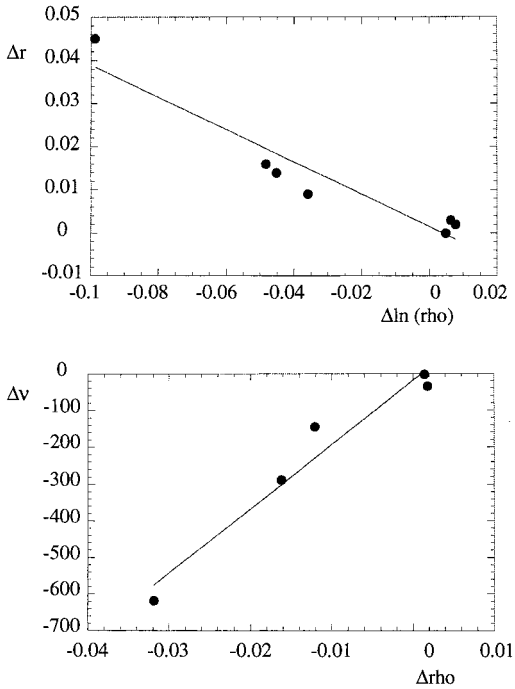

Figure 4. Representation of (top) the change in the bond length of the X−H bonds (Δ*r*; Å) involved in intermolecular contacts vs the variation in the logarithm of the electron density and (bottom) the stretching frequency shift (cm^{-1}) vs the variation in the electron density (ua) at the corresponding bond critical points.

N6−H6 (AU). Indeed, the largest the electron density depletion, the greatest the changes experienced in bond length and red shift. However, in C−H bonds there is an increase in the electron density upon complexation, and this effect is larger as the interatomic distance becomes shorter (the magnitude of this effect decrease in the order C5−H5 (UU7) ∼ C5−H5 (UU−C) > C2−H2 (AU)). This different behavior likely stems from the different nature of stabilizing forces in intermolecular contacts involving N−H or C−H bonds, since the former are expected to be dominated by electrostatics, whereas dispersion is more important in the latter.

For our purposes here, the preceding results suggests that the C−H···O contacts in AU and UU pairs exert different contributions to the stabilization of the corresponding complexes. Thus, the C2−H2···O2 bond in the AU pair is expected to be sensibly less stabilizing than the C5−H5···O2 and C5−H5···O4 bonds in the UU pairs. Indeed, the changes in the integrated atomic properties of the hydrogen atom in the C2−H2 bond in the AU pair are clearly smaller than those observed for the hydrogen atoms of the C5−H5 bonds in the UU dimers. Overall, whereas the C5−H5···O hydrogen bond contributes to the formation of the uracil dimers, the results allow us to argue against a significant role of the C2−H2···O2 contact in stabilizing the AU WC pair.

3.3. Natural Bond Orbital Analysis. *AU WC Base Pair.* Analyzing the NBO densitites, we found an electron density transfer (EDT) of 318 me from adenine to uracil. Investigating individual densities, we found the largest EDT from the adenine N1 lone electron pairs to the thymine N3−H3 σ^* antibonding orbital (649 me) and from the thymine O4 lone electron pairs to the adenine N6−H61 σ^* antibonding orbital (265 me). Summing these two EDTs, one obtains an EDT of 384 me from adenine to thymine what is close to the total EDT of 318 me. In both cases we obtain an electron density increase in the X−H σ^* antibonding orbitals which results in weakening of these bonds, their elongation, and a concomitant red shift of their strech frequencies. Evidently, N1···H3−N3 as well as O4···H61−N6 contacts correspond to standard H-bonding. The situation is different in the case of the O2···H2−C2 contact. The electron density in the adenine C2−H2 σ^* antibonding orbital is not changed upon formation of a pair which excludes formation of the respective H-bond as well as improper H-bond. This is also supported by the net change of the thymine O2 natural charge that becomes slightly more negative upon formation of a pair. Let us recall that existence of an H-bond as well as an improper H-bond of the X−H···Y type is connected with electron density decrease at the proton acceptor (Y).

UU Pairs. From the NBO densities of UU7 pair it follows that electron density is transferred from the uracil acting as C−H proton donor to the other one. The total EDT (287 me) is slightly smaller than that in AU WC. Analyzing the electron densities in the N−H···O contact, we found electron density decrease at the O4 lone electron pairs and a large electron density increase

(38 me) in the N1−H1 σ^* antibonding orbital. In the case of the C−H...O contact we detected again an electron density increase (13 me) in the C5−H5 σ^* antibonding orbital, but here electron density at the O2 lone electron pairs slightly increases (by 2 me). Electron density increase in N1−H1 and C5−H5 σ^* antibonding orbitals leads to weakening of both bonds, their elongation, and a concomitant red shift of the respective strech vibration frequencies. Though the EDT to C5−H5 antibonding orbital is smaller than that to N1−H1, this gives clear evidence about formation of the standard (though weak) H-bond of the C−H···O type. The situation in the UU−C pair is similar. Also here we found a rather strong N1−H···O4 H-bond characteristic by increase of electron density in the N1−H σ^* antibonding orbital (33 me) which is accompanied by the N1−H bond length increase. The C5−H···O2 contact corresponds also to an H-bond, which is, however, weaker. The electron density in the σ* antibonding orbital increases by 12 me which is accompanied by bond length increase.

4. Conclusion

Harmonic vibrational analysis performed at the correlated MP2 level reveals two H-bonds of N−H···N and N−H···O types in the AU WC base pairs while no support is given to existence of the third bond, either C−H···O H-bond or improper, blue-shifting H-bond. The H2 adenine hydrogen does not play any active role in the pairing. On the other hand, the vibrational analysis shows two H-bonds of N−H···O and C−H···O types in the UU7 base pair. Vibrational analysis results agreed with atom-in-molecule Bader analysis of electron density and with natural bond orbital analysis. It is thus possible to conclude that there are two strong H-bonds in the AU WC pair and one strong and one weaker H-bonds in both UU pairs. The existence of the third H-bond in the AU pair was ruled out, which fully agrees with recently published results obtained using HF and density functional theory methods.[32]

Acknowledgment. We thank Prof. R. W. F. Bader for sending us a copy of the PROAIM computer program. This study was supported by Grants 203/98/1166 and 203/00/0633 from the Grant Agency of the Czech Republic and by Grants PB98-1222 and PB96-1005 from the Spanish DGICYT. We also thank the Centre de Supercomputació de Catalunya (CESCA; Molecular Recognition project) and the Supercomputer Center, Brno, Czech Republic, for computational facilities.

References and Notes

(1) Jeffrey, G. A. *An Introduction to Hydrogen Bonding*; Oxford University Press: New York, 1997.

(2) Scheiner, S. *Hydrogen Bonding. A Theoretical Perspective*; Oxford University Press: New York, 1997.

(3) Pribble, R. N.; Garret, A. W.; Haber, K.; Zwier, T. S. *J. Chem. Phys*. **1995**, *103*, 10573.

(4) Djafari, S.; Lembach, G.; Barth, H.-D.; Brutschy, B. *J. Chem. Phys*. **1997**, *107*, 10573.

(5) Alkorta, I.; Rozas, I.; Elguero, J. *Chem. Soc. Rev*. **1998**, *27*, 163.

(6) Taylor, R.; Kennard, O. *J. Am. Chem.. Soc*. **1982**, *104*, 5063.

(7) (a) Steiner, T.; et al. *J. Chem. Soc., Perkin Trans. 2* **1996**, 2441. (b) Desiraju, G. R.; Steiner, T. *The Weak Hydrogen Bond*; Oxford University Press: Oxford, U.K, 1999.

(8) Hobza, P.; Špirko, V.; Selzle, H. L.; Schlag, E. W. *J. Phys. Chem. A* **1998**, *102*, 2501.

(9) Hobza, P.; Špirko, V.; Havlas, Y.; Buchhold, K.; Reinmann, B.; Barth, H.-D.; Brutschy, B. *Chem. Phys. Lett.* **1999**, *299*, 553.

(10) (a) Bader, R. F. W. *Atoms in Molecules. A Quantum Theory*; Oxford University Press: Oxford, U.K., 1990. (b) Bader, R. F. W. *Chem. Rev.* **1991**, *91*, 893. (c) Bader, R. F. W. *J. Phys. Chem. A* **1998**, *102*, 7314.

(11) Cubero, E.; Orozco, M.; Hobza, P.; Luque, F. J. *J. Phys. Chem. A* **1999**, *103*, 6394.

(12) Hobza, P.; Havlas, Z. *Chem. Phys. Lett*. **1999**, *303*, 447.

(13) Cubero, E.; Orozco, M.; Luque, F. J. *Chem. Phys. Lett*. **1999**, *310*, 445.

(14) Weber, J. M.; Kelley, J. A.; Robertson, W. H.; Lisle, K. M.; Johnson, M. A.; Havlas, Z.; Hobza, P. *J. Am. Chem. Soc*., submitted for publication.

(15) Reed, A. E.; Curtiss, L. A.; Weinhold, F. *Chem. Rev*. **1988**, *88*, 899.

(16) Wahl, M. C.; Sundaralingam, M. *Trends Biochem. Sci*. **1997**, *22*, 97.

(17) Leonard, G. A.; McAuley-Hecht; Brown, T.; Hunter, W. N. *Acta Cryst*allogr. **1995**, *D51*, 136.

(18) Starikov, E. B.; Steiner, T. *Acta Crystallogr*. **1997**, *D53*, 345.

(19) Kratochvíl, M.; Engkvist, O.; Šponer, J.; Jungwirth, P.; Hobza, P. *J. Phys. Chem. A* **1998**, *102*, 6921.

(20) Hariharan, P. C.; Pople, J. A. *Theor. Chim. Acta* **1973**, *28*, 213.

(21) Boys, S. F.; Bernardi, F. *Mol. Phys*. **1970**, *19*, 553.

(22) Hobza, P.; Havlas, Z. *Theor. Chim. Acta* **1998**, *99*, 372. Simon, S.; Duran, M.; Dannenberg, J. J. *J. Chem. Phys*. **1996**, *105*, 11024.

(23) Špirko, V.; Šponer, J.; Hobza P. *J. Chem. Phys*. **1997**, *106*, 1472.

(24) Frisch, M. J.; Trucks, G. W.; Schlegel, H. B.; Gill, P. M. W.; Johnson, B. G.; Robb, M. A.; Cheeseman, J. R.; Keith, T. A.; Petersson, G. A.; Montgomery, J. A.; Raghavachari, K.; Al-Laham, M. A.; Zakrzewski, V. G.; Ortiz, J. V.; Foresman, J. B.; Cioslowski, J.; Stefanov, B. B.; Nanayakkara, A.; Challacombe, M.; Peng, C. Y.; Ayala, P. Y.; Chen, W.; Wong, M. W.; Andres, J. L.; Replogle, E. S.; Gomperts, R.; Martin, R. L.; Fox, D. J.; Binkley, J. S.; Defrees, D. J.; Baker, J.; Stewart, J. P.; Head-Gordon, M.; Gonzalez, C.; Pople, J. A. *Gaussian 94, Rev. A.1*; Gaussian Inc.: Pittsburgh, PA, 1995.

(25) Frisch, M. J.; Trucks, G. W.; Schlegel, H. B.; Scuseria, G. E.; Robb, M. A.; Cheeseman, J.; Zakrzewski, R.; Montgomery Jr., J. A.; Stratmann, R. E.; Burant, J. C.; Dapprich, S.; Millam, J. M.; Daniels, A. D.; Kudin, K. N.; Strain, M. C.; Farkas, O.; Tomasi, J.; Barone, V.; Cossi, M.; Cammi, R.; Mennucci, B.; Pomelli, C.; Adamo, C.; Clifford, S.; Ochterski, J.; Petersson, G. A.; Ayala, P. Y.; Cui, Q.; Morokuma, K.; Malick, D. K.; Rabuck, A. D.; Raghavachari, K.; Foresman, J. B.; Cioslowski, J.; Ortiz, J. V.; Stefanov, B. B.; Liu, G.; Liashenko, A.; Piskorz, P.; Komaromi, I.; Gomperts, R.; Martin, R. L.; Fox, D. J.; Keith, T.; Al-Laham, M. A.; Peng, C. Y.; Nanayakkara, A.; Gonzalez, C.; Challacombe, M.; Gill, P. M. W.; Johnson, B.; Chen, W.; Wong, M. W.; Andres, J. L.; Head-Gordon, M.; Replogle, E. S.; Pople, J. A. *Gaussian 98, Rev. A.7*; Gaussian Inc.: Pittsburgh, PA, 1999.

(26) (a) Popelier, P. L. A. *J. Phys. Chem A* **1998**, *102*, 1873. (b) Carroll, M. T.; Chang, C.; Bader, R. F. W. *Mol. Phys*. **1988**, *65*, 695. (c) Destro, R.; Biachi, R.; Gatti, C.; Merati, F. *Chem. Phys. Lett*. **1991**, *47*, 186. (d) Alkorta, I.; Elguero, J. *J. Phys. Chem. A* **1999**, *103*, 272. (e) Rozas, I.; Alkorta, I.; Elguero, J. *J. Phys. Chem. A* **1998**, *102*, 9925. (f) Luque, F. J.; Lopez, J. M.; Lopez de Paz, M.; Vicent, C.; Orozco, M. *J. Phys. Chem. A* **1998**, *102*, 6690. (g) Cubero, E.; Orozco, M.; Luque, F. J. *J. Phys. Chem. A* **1999**, *103*, 315.

(27) Biegler-Kšnig, F.; Bader, R. F. W.; Tang, T. H. J. *Comput. Chem.* **1982**, *3*, 317.

(28) (a) Hobza, P.; Šponer, J.; Polásek, M. *J. Am. Chem. Soc*. **1995**, *117*, 792. (b) Šponer, J.; Leszczynski, J.; Hobza P. *J. Phys. Chem*. 1996, *100*, 1965. (c) Hobza, P.; Šponer, J. *Chem. Phys. Lett*. **1998**, *288*, 7.

(29) Kock, U., Popelier, P. L. A. *J. Phys. Chem*. **1995**, *99*, 9747.

(30) (a) Alkorta, I.; Rozas, I.; Elguero, J. *Struct. Chem*. **1998**, *9*, 243. (b) Alkorta, I.; Rozas, I.; Elguero, J. *J. Mol. Struct. (THEOCHEM)* **1998**, *452*, 227. (c) Alkorta, I., Elguero, J. *J. Phys. Chem. A* **1999**, *103*, 272.

(31) (a) Boyd, R. J.; Choi, S. C. *Chem. Phys. Lett*. **1985**, *120*, 80. (b) Boyd, R. J.; Choi, S. C. **1986**, *129*, 62. (c) Bader, R. F. W.; Tang, T. H.; Tal, Y.; Biegler-Kšnig, F. *J. Am. Chem. Soc*. **1982**, *104*, 946. (d) Mallinson, P. R.; Wozniak, K.; Smith, G. T.; McCormack, K. L. *J. Am. Chem. Soc*. **1997**, *119*, 11502. (e) Roversi, P.; Barzaghi, M.; Merati, F.; Destro, R. *Can. J. Chem*. **1996**, *74*, 1145.

(32) Šponer, J.; Leszczynski, J.; Hobza, P. *J. Phys. Chem. A* **1997**, *101*, 9489 (b) Shishkin, O. V.; Šponer, J.; Hobza, P. *J. Mol. Struct*. **1999**, *477*, 15. (c) Guerra, C. F.; Bickelhaupt, F. M.; Snijders, J. G.; Baerends, E. J. *Eur. J. Chem*. **1999**, *5*, 3581.

(Esta página está intencionadamente en blanco)

4.3 Interacciones canónicas con bases modificadas[1,11]

Las bases modificadas han sido ampliamente utilizadas en la última década[11]. Su uso ha permitido la comprensión de la estabilidad de los ácidos nucleicos, el estudio del mecanismo de reconocimiento molecular entre las bases, etc[12,13]. La modificación de las bases puede acentuar o atenuar propiedades ya existentes, o bien puede otorgar nuevas propiedades, que pueden utilizarse en aplicaciones biotecnológicas o biomédicas[14].

Incrementar el número de interacciones por puentes de hidrógeno o el uso de análogos no polares son sólo algunas de las principales estrategias[11,15] utilizadas en el diseño de pseudobases con el fin de obtener una mayor estabilización de las estructuras de los ácidos nucleicos.

En el apartado 4.3.1 se ha estudiado el efecto de los grupos amino unidos a la posición 2 y 8 de la hipoxantina sobre la estructura, la estabilidad y la reactividad de dúplexes y tríplexes de ADN mediante simulaciones de dinámica molecular (MD) e integración termodinámica (TI)[16] y cálculos de mecánica cuántica (QM)[17,18].

La síntesis química de las bases modificadas y de los oligonucleótidos, los experimentos de fusión y los posteriores análisis termodinámicos de los cambios en dúplexes y tríplexes cuando la 2-deoxinosina es mutada a la 2-deoxiguanosina y a la 8-amino-2-deoxinosina han sido realizados por el grupo del Dr. R. Eritja.

En los apartados 4.3.2 y 4.3.3 se ha estudiado un isóstero no polar de la timina (T), el difluorotolueno (F). Esta base tiene la misma forma que el correspondiente nucleósido natural, pero carece de capacidad para formar puentes de hidrógeno[19]. Experimentalmente, se conoce que el ADN polimerasa I incorpora difluorotolueno frente adenina (A) y adenina frente al difluorotolueno con una elevada precisión[20]. También se sabe que dúplexes que contienen difluorotolueno son estables, aunque menos que el correspondiente dúplex canónico[21].

En el apartado 4.3.2 se presenta el resultado de una extensa dinámica molecular (MD)[16] de dos oligonucleótidos que contienen el par de bases A·F y el par canónico A·T. Con la finalidad de complementar estos estudios de MD, se ha determinado la termodinámica de formación de los dímeros mediante técnicas QM[17].

En el apartado 4.3.3 se determinan los cambios estructurales y energéticos en el ADN que acompañan a la sustitución de timina por difluorotolueno. Se han estudiado varias estructuras de doble hélice, que contienen el dímero A·F o A·T, y de triple hélice, que contienen la tríada (A·T)·T o (A·F)·T o (A·T)·F, mediante técnicas de dinámica molecular (MD) e integración termodinámica (TI)[16].

4.3.1 The effect of amino groups on the stability of DNA duplexes and triplexes based on purines derived from inosine

Elena Cubero, Ramón Güimil-García, F. Javier Luque, Ramón Eritja & Modesto Orozco

Nucleic Acids Res. **2001**, *29*, 2522-2534

(Esta página está intencionadamente en blanco)